Available online at www.sciencedirect.com

ScienceDirect

Nuclear Physics A 987 (2019) 46–78

NUCLEAR PHYSICS A

www.elsevier.com/locate/nuclphysa

Radiative ^{3}He(^{2}H, γ)^{5}Li capture at astrophysical energy and its role in accumulation of ^{6}Li at the BBN

S.B. Dubovichenko [a,b,*], N.A. Burkova [b], A.V. Dzhazairov-Kakhramanov [a,**], R.Ya. Kezerashvili [c,d], Ch.T. Omarov [a], A.S. Tkachenko [a,b], D.M. Zazulin [b,e]

[a] *Fesenkov Astrophysical Institute "NCSRT" ASA MDASI RK, 050020, Almaty, Kazakhstan*
[b] *al-Farabi Kazakh National University, 050040, Almaty, Kazakhstan*
[c] *Physics Department, New York City College of Technology, City University of New York, 300 Jay Street, Brooklyn, New York 11201, USA*
[d] *Graduate School and University Center, City University of New York, New York 10016, USA*
[e] *Institute of Nuclear Physics, ME RK, 050032, Almaty, Kazakhstan*

Received 21 February 2019; received in revised form 24 March 2019; accepted 28 March 2019
Available online 11 April 2019

Abstract

Big Bang Nucleosynthesis (BBN) relevance reactions ^{3}He(^{2}H, γ)^{5}Li, ^{3}H(^{3}He, γ)^{6}Li, and ^{5}Li(n, γ)^{6}Li as a key to approach for scenario of ^{6}Li formation are treated. The rates of reaction for these processes are analyzed. Comparison of the reactions rates and the prevalence of light elements leads to the assumption that the two-step process $^{2}\mathrm{H} + {}^{3}\mathrm{He} \rightarrow {}^{5}\mathrm{Li} + \gamma$ and $n + {}^{5}\mathrm{Li} \rightarrow {}^{6}\mathrm{Li} + \gamma$ can make a significant contribution to the formation of ^{6}Li at the BBN at least at temperatures T_9 of the order of unity. Calculations of the total cross sections, astrophysical S-factor, and reaction rates have been performed for ^{3}He(^{2}H, γ)^{5}Li radiative capture within the modified potential cluster model with forbidden states, which follow from the classification of the orbital cluster states according to Young diagrams. Numerical data and corresponding parametrizations cover the energy range up to 5 MeV and temperature range $T_9 < 10$. An updated compilation of detailed data for the reaction ^{3}He(^{2}H, γ)^{5}Li are presented.

* Corresponding author at: Fesenkov Astrophysical Institute "NCSRT" ASA MDASI RK, 050020, Almaty, Kazakhstan.
** Corresponding author.
E-mail addresses: dubovichenko@mail.ru (S.B. Dubovichenko), albert-j@yandex.ru (A.V. Dzhazairov-Kakhramanov).

https://doi.org/10.1016/j.nuclphysa.2019.03.017
0375-9474/

Keywords: Light nuclei; Astrophysical factor; Radiative capture; Cluster model; Reaction rate

1. Introduction

The interest to the radiative capture reactions in the isobar-analogue channels ^{3}He(^{2}H, γ)^{5}Li and ^{3}H(^{2}H, γ)^{5}He is primarily due to the following two reasons: these reactions are parts of nucleosynthesis chain of the processes occurring in the early stages of a stable star formation, as well as possible candidates for the overcoming of the well-known problem of the $A = 5$ gap in the synthesis of light elements in the primordial Universe [1] and application of these processes for the diagnostics of nuclear fusion efficiencies of ^{2}H(^{3}H, n)^{4}He and ^{2}H(^{3}He, p)^{4}He reactions used for experimental studies of tokamak plasmas [2,3].

It is believed that the ^{3}He(^{2}H, γ)^{5}Li process is well studied experimentally. Since 1954 [4] a sufficient number of experimental works, see, for example, Refs. [5–9] are devoted to study this process, and the most recent data are presented in Ref. [10], including compilations of experimental data on cross sections, astrophysical factors and rates of this reaction at energies less than 200 keV [3,11]. However, in our opinion, the experimental and theoretical situation is far from unambiguous and requires systematic analysis, which we implement in this article relying as a certain criterion on our model theoretical calculations.

There is another "unambiguous" opinion: due to the smallness of the cross section the ^{3}He(^{2}H, γ)^{5}Li reaction does not contribute to the astrophysical processes [12]. In this paper we address this issue and demonstrate that this statement is disputable, since the rate of this reaction is not negligible. In addition, we will consider a possible scenario for astrophysical processes of ^{6}Li formation involving a short-lived ^{5}Li isotope.

In this paper, the radiative ^{3}He(^{2}H, γ)^{5}Li capture is considered on the basis of the modified potential cluster model (MPCM) and renewed results are obtained for dipole $E1$ and $M1$ transitions, taking into account the mixing of the doublet and quartet spin channels, for both the scattering and the bound ground states. We construct the potentials of the intercluster interaction based on the description of the known scattering phase shifts and the main characteristics of the ground state (GS) of ^{5}Li. The total cross sections for the ^{3}He(^{2}H, γ)^{5}Li capture rate into the GS of ^{5}Li at energies in the frame of the center-of-mass (c.m.) from 5 keV to 5 MeV are calculated. Finally, we propose simple analytic parametrizations for the astrophysical S-factor and the rate of this reaction.

The parametrization of the cross sections for the ^{3}H(^{3}He, γ)^{6}Li and ^{5}Li(n, γ)^{6}Li processes of radiative capture is carried out. The rates corresponding to these processes are calculated, their parametrization is performed, and a comparison with the ^{3}He(^{2}H, γ)^{5}Li and ^{4}He(^{2}H, γ)^{6}Li capture reactions rate are made. On the basis of comparisons of the rates of these reactions and the prevalence of light elements, we suggests that the two-step process $^2\mathrm{H} + {}^3\mathrm{He} \to {}^5\mathrm{Li} + \gamma$ and $n + {}^5\mathrm{Li} + \gamma \to {}^6\mathrm{Li} + \gamma$ can make a certain contribution to the production of ^{6}Li at the BBN at least at temperatures T_9 of the order of unity. In this temperature range the number of neutrons does not yet begin to decrease, while the number of ^{2}H and ^{3}He nuclei is already reaching its maximum, which leads to increase in the reaction yield $^2\mathrm{H} + {}^3\mathrm{He} \to {}^5\mathrm{Li} + \gamma$.

This paper is organized in the following way. In Sec. 2 we review of experimental results and discuss the application range of the ^{3}He(^{2}H, γ)^{5}Li capture reaction. The model, methods of calculation and potentials for elastic ^{2}H^{3}He scattering and ^{2}H^{3}He bound states are presented in Sec. 3. In Sec. 4 results of calculations for total cross sections, astrophysical S-factor and reaction rate are presented and discussed. In Sec. 5 the two-step process $^2\mathrm{H} + {}^3\mathrm{He} \to {}^5\mathrm{Li} + \gamma$

and $n + {}^5\mathrm{Li} + \gamma \rightarrow {}^6\mathrm{Li} + \gamma$ is considered and discussed as an alternative way of the formation of ^{6}Li at the BBN. Conclusions follow in Sec. 6.

2. Application of the ^{3}He(^{2}H, γ)^{5}Li and review of experimental results

Let us now examine in more detail the various aspects of the ^{3}He(^{2}H, γ)^{5}Li reaction, including the experimental data presented in the data base of EXFOR [13] and the original papers cited therein and the role of this process in various fields of application.

2.1. Nuclear astrophysics aspects

Our parametrization of the experimental data for ^{2}H capture in ^{3}He [7] for the S-factor at energies from 0.2 to 1.0 MeV according to Breit-Wigner and its further extrapolation to zero energy leads to a value of 0.24 keV·b. Let us give for comparison several known values of the S-factors at zero energy for some radiative capture reactions. For example, the latest data for the astrophysical factor of the proton capture on ^{2}H give the value $S(0) = 0.216(11)\cdot10^{-3}$ keV·b [14], while in Ref. [15] is reported $S(0) = 0.166(14)\cdot10^{-3}$ keV·b. At the same time, for the proton capture in ^{3}H, $S(0) = 2.0(2)\cdot10^{-3}$ keV·b [16], i.e. an order of magnitude greater. Measurements in Ref. [17], lead to $S(0) = 1.3(3)$ keV·b and $S(0) = 6.0(1.2)\cdot10^{-6}$ keV·b for ^{3}H(^{2}H, γ)^{5}He and ^{2}H(^{2}H, γ)^{4}He capture, respectively. The S-factor for ^{2}H(^{2}H, γ)^{4}He capture is smaller due to the strong $E1$ transition in this process, which is forbidden due to equal masses of the particles in the initial channel [3].

In Ref. [17], 0.36(9) keV·b is given for the astrophysical factor of the ^{3}He(^{2}H, γ)^{5}Li capture. At the same time, more recent results [11] for the ^{3}He(^{2}H, γ)^{5}Li capture, the S-factor is $S(0) = 0.26(7)$ keV·b, which is in a good agreement with our value of 0.24 keV·b, which we report below. Although the error bands of these data [11] and [17] overlap, in fact, the values of the astrophysical factor of this reaction can be in the range 0.19–0.45 keV·b. This is a very large uncertainty for its values, which leads, despite the relatively low abundance of ^{3}He, to the rather large uncertainty of the contribution of the reaction under consideration to the primordial nucleosynthesis of the Universe and the processes of initial star formation.

Therefore, a more detailed study of this process will allow to obtain the results for the reaction rate and to compare it with the rates of other reactions of thermonuclear fusion, given, for example, by [12]. This work contains simple parameterizations of rates for dozens of thermonuclear reactions, but there are no data for ^{3}He(^{2}H, γ)^{5}Li capture. Perhaps this is due to the fact that the rate of the reaction under study was considered to be negligible. However, below we show that the rate of this reaction at certain temperatures is larger than the rate of proton capture on ^{2}H and is comparable with the rate of proton capture on ^{3}H. Thus, the ^{3}He(^{2}H, γ)^{5}Li reaction rate among the rates of the processes of radiative capture in the considered temperature range of 0.01–10.0 T_9 is actually of the similar magnitude to the other processes which are considered as an important.

2.2. Nuclear physics aspects and experimental results

Let us present a survey of experimental measurements of the total cross sections of the ^{3}He(^{2}H, γ)^{5}Li capture as well as our estimation of the total cross section obtained from the measurements of differential cross sections and the polarization characteristics. From the point of view of nuclear physics, practically all experimental studies of the total cross sections of

Table 1
Energy levels for ^{5}Li and ^{5}He. The table is based on the data from Ref. [18]. E_x is excitation energy, in MeV, referred to the ground state GS and J^π is the angular momentum and parity.

Energy levels of ^{5}He		Energy levels of ^{5}Li	
E_x (MeV)	J^π, T	E_x (MeV)	J^π, T
GS	$\frac{3}{2}^-; \frac{1}{2}$	GS	$\frac{3}{2}^-; \frac{1}{2}$
1.27	$\frac{1}{2}^-; \frac{1}{2}$	1.49	$\frac{1}{2}^-; \frac{1}{2}$
16.84	$\frac{3}{2}^+; \frac{1}{2}$	16.87	$\frac{3}{2}^+; \frac{1}{2}$
19.14	$\frac{5}{2}^+; \frac{1}{2}$	19.28	$\frac{3}{2}^-; \frac{1}{2}$
19.26	$\frac{3}{2}^+; \frac{1}{2}$	19.45	$\frac{7}{2}^+; \frac{1}{2}$
19.31	$\frac{7}{2}^+; \frac{1}{2}$	19.71	$\frac{5}{2}^+; \frac{1}{2}$
19.96	$\frac{3}{2}^-; \frac{1}{2}$	20.53	$\frac{1}{2}^+; \frac{1}{2}$
21.25	$\frac{3}{2}^+; \frac{1}{2}$	22.06	$\frac{5}{2}^-; \frac{1}{2}$
21.39	$\frac{5}{2}^+; \frac{1}{2}$	23.74	$\frac{5}{2}^+; \frac{1}{2}$
21.64	$\frac{1}{2}^+; \frac{1}{2}$	25.42	$\frac{3}{2}^+; \frac{1}{2}$
23.97	$\frac{7}{2}^+; \frac{1}{2}$	25.44	$\frac{7}{2}^+; \frac{1}{2}$
24.06	$\frac{5}{2}^-; \frac{1}{2}$	32.53	$\frac{1}{2}^-; \frac{1}{2}$

^{3}He(^{2}H, γ)^{5}Li reaction for capturing to the ground state of ^{5}Li from the 1960s to the present are limited to two works published in late 1960s and early 1970s [7,8]. Only in these works the total cross sections of the radiative ^{3}He(^{2}H, γ)^{5}Li capture at the astrophysical energy range are shown in an explicit form.

The energy levels for ^{5}He and ^{5}Li are published in Ref. [18]. However, the published version has been corrected and updated by the authors later (see [18]). In Table 1 we present the summary of the energy levels for ^{5}He and ^{5}Li isotopes. In Ref. [7] measurements were made at a deuteron energy of 200–1360 keV in the laboratory system (l.s.). For the ^{3}He(^{2}H, γ)^{5}Li reaction separation of the transitions into the GS and the first excited state (FES) of ^{5}Li (see Table 1) have been studied. However, as a result of the poor quality of the experimental data for the transition to the FES of ^{5}Li, the integral cross sections are presented only for the transition to the ground state with a value of 21(4) μb for $\sigma_{\gamma 0,\mathrm{cm}}$ at $E_R = E_{\mathrm{cm}} = 0.27$ MeV [7]. The angular distributions measured in [7] at $E_{\mathrm{cm}} = 0.288$ and 0.615 MeV for the transition to the ground state of ^{5}Li was consistent with isotropy to within 10%. The total cross sections obtained in [7] with an accuracy of 20% are shown below in Fig. 1.

In Ref. [8] the total cross sections were measured at excitation energy E_x from 17.4 to 21.1 MeV. If we use the binding energy for the ^{2}H^{3}He channel of 16.66 MeV [18], we obtain capture energy of 0.74–4.44 MeV in the c.m. In Ref. [8] the value of the binding energy of 16.4 MeV was used, which is close to 16.39 MeV given in Ref. [19]. Using energy of 16.4 MeV, we obtain capture energy of 1.0–4.7 MeV in the c.m. These values will be used throughout our work.

The capture total cross sections obtained in Ref. [8] have a wide maximum (the width of 3–4 MeV) with the value of 59(3.0) μb at the energy $E_x = 19.7$ MeV, i.e. at 3.3 MeV in the c.m. This maximum points at the existing group of broad levels in this energy range. This group of levels at energies 19.28–22.06 MeV clearly can be identified in the spectra of ^{5}Li shown in Table 1. The total cross sections for capture into the GS obtained in [8] are shown in Fig. 1. The angular

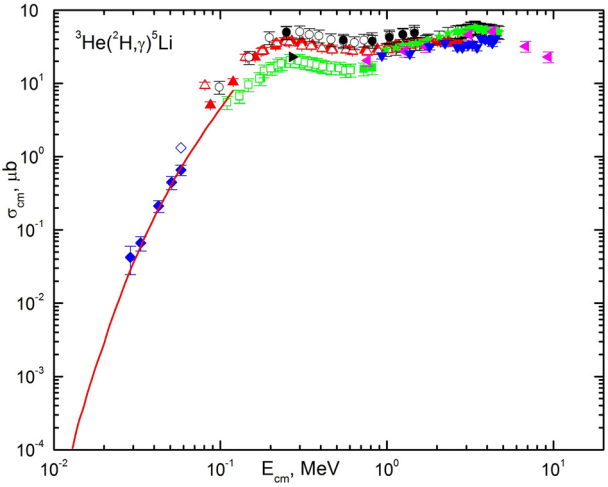

Fig. 1. The total cross sections of the ^{3}He(^{2}H, γ)^{5}Li capture. The experimental data □ and ■ – from Ref. [7] for γ_0 and ★ – are from Ref. [8]. The other data are recounted by us from some reference, namely: ○ and ● – from Ref. [4] for $\gamma_0 + \gamma_1$, △ and ▲ – from Ref. [5] for γ_0, ▼ – from Ref. [6] for $\gamma_0 + \gamma_1$, for γ_0, ◄ – from Ref. [20] for γ_0, ◆ for γ_0 and ◇ for γ_1 – from Refs. [24,25], ► – from Refs. [9,10] for γ_0, and the solid curve from Ref. [11] for γ_0.

distributions at angles $\theta_{\gamma,\mathrm{lab}} = 0°–130°$ obtained in Ref. [18] for the transition to the GS of ^{5}Li are close to the isotropic up to the energy of 4 MeV in c.m. The statistical error of the data obtained in [8] was 5%, but due to the high uncertainty of the procedure of separating the peaks from the transitions to the ground and first excited states of ^{5}Li the error in the determination of the absolute values of the cross sections can reach up to 40%.

Once again we note that the most complete databases of nuclear data such as EXFOR [13], as well as well-known atomic characteristics databases, for example, PHYSICS, CDFE, NASA DATA [21,22], contain only these data for total cross sections of ^{3}He(^{2}H, γ)^{5}Li capture at low energies. Besides them, however, there are several publications [4–6,9,10,20] in which measurements of the number of events observed in experiments with a polarized beam and differential capture cross sections are realized. Therefore, we perform a recalculation of some of the experimental measurements of these studies with the extraction of the total cross sections from them. Let us now explore in more detail on the experimental aspects of above mentioned studies and make a comparison of the total cross sections obtained with their help.

Probably, for the first time, the yields of the ^{3}He(^{2}H, γ)^{5}Li reaction at low energies were measured by Blair et al. [4] back in 1954. It was assumed that the reaction proceeds with capture to the ground and first excited states of the nucleus. However, due to the insufficient energy resolution, the peaks from these transitions could not be separated and as a result the total yield from all possible transitions was presented. The excitation function obtained for $\theta_{\gamma,\mathrm{lab}} = 90°$ and $E_{\mathrm{cm}} = 0.1–1.5$ MeV showed a wide resonance at $E_{\mathrm{cm}} = 0.27$ MeV with a total cross section in the peak equal to 50(10) μb. Also authors of Ref. [4], measured the angular distribution of the total yield of the reaction at $E_{\mathrm{cm}} = 0.35$ MeV, which turned out to be isotropic with an accuracy of 10%. To obtain the integral cross sections from the data of [4] the yield of this reaction, shown in Fig. 3 in this work was normalized to the total cross section measured at the resonance energy $E_R = E_{\mathrm{cm}} = 0.27$ MeV. In Fig. 1 are presented the integral cross sections, which we recalculated from the yield of the ^{3}He(^{2}H, γ)^{5}Li reaction given in [4].

Subsequently, in [5], the differential cross sections of the ^{3}He(^{2}H, γ)^{5}Li reaction for $\theta_{\gamma,\text{lab}} = 90°$ were measured in the energy range $E_{\text{cm}} = 0.08$–2.76 MeV. Authors of Ref. [5] could not find any indications of the presence of a peak from the transition to the first excited state of ^{5}Li in the spectra of the ^{3}He(^{2}H, γ)^{5}Li reaction, and the single broad peak in the spectra was interpreted as the peak from the transition to the ground state of ^{5}Li. However, it is possible that this broad peak contained also the transition to the first excited state of ^{5}Li but the accuracy of the experiment did not allow one to distinguish it. The measurement of the angular distributions at $E_{\text{cm}} = 0.3$ and 1.66 MeV with 7% error reported in Ref. [5] also turned out to be isotropic. The integral cross section obtained in Ref. [5] for ^{3}He(^{2}H, γ)^{5}Li at the resonance energy $E_R = E_{\text{cm}} = 0.27$ MeV is 38(4) μb.

Furthermore, in Ref. [6] the sum of the differential cross sections of the reaction ^{2}H(^{3}He, γ)^{5}Li for the transitions to the ground and first excited states of ^{5}Li at $\theta_{\gamma,\text{lab.}} = 90°$ in the energy range of $E_{\text{cm}} = 0.93$–4.5 MeV were measured. The obtained excitation function, accurate to within 10% of the measurement demonstrates a smooth growth with increasing energy without a clear indication of the presence of any resonances of the reaction ^{2}H(^{3}He, γ)^{5}Li in the considered energy range. When we obtained the integral cross sections from the data of [5,6], the differential cross sections shown in Fig. 5 of Ref. [5] and Fig. 2 of Ref. [6] were simply multiplied by 4π (here we assume the isotropy in the angular distributions that was shown in all works listed above) and these results are shown in Fig. 1. It can be seen from Fig. 1 that the data of [5] differ quite strongly from the measurements [7], although in both cases it is said that capture is only to the GS of ^{5}Li. In addition, the results of [6] for capture to the GS and FES lie below the cross sections of Ref. [8] obtained for the capture to the GS.

Somewhat later in Ref. [20] the excitation functions of the reaction ^{2}H(^{3}He, γ)^{5}Li at $\theta_{\gamma,\text{lab}} = 90°$ and $E_{\text{cm}} = 0.76$–10.1 MeV for transitions to the ground and first excited states of ^{5}Li were obtained. Moreover, in Ref. [20] the sum of the differential cross sections for the transitions to the ground and first excited states of ^{5}Li at $\theta_{\gamma,\text{lab}} = 90°$ is given. For five energies, the angular distributions for these transitions were measured. Work [20] presented a table with the ratios of the coefficients of the Legendre functions of A_2/A_0 and A_1/A_0 for the cases when the first two and first three terms of the expansion in describing these angular distributions are taking into account. The error in determining the absolute values of the cross sections without taking into account the error in the procedure of separating of the peaks from the two transitions was 17%. A change of the angular distributions with the energy and the form of the excitation functions of the ^{2}H(^{3}He, γ)^{5}Li reaction allowed the authors of Ref. [20] to make a conclusion about the existence of a broad resonance structure with the width of 3–4 MeV in the range of $E_{\text{cm}} = 0.76$–10.1 MeV and the maximum $\sigma_{\gamma 0} = 51(8)$ μb located at $E_{\text{cm}} \approx 4.3$ MeV. Using data [20], we obtained the values of the integral cross section for $E_{\text{cm}} = 0.764$, 1.282, 1.712, 3.112, 4.312, 6.812, 9.312 MeV only for capture to the ground state of ^{5}Li, since the data of [20] for the first excited state of ^{5}Li are unreadable due to the error of the order of 100%. We obtain the cross section for the energies $E_{\text{cm}} = 0.764$, 1.282, and 1.712 MeV, by simply multiplying the differential cross sections [20], taken from Fig. 8 of this work by 4π, since at these energies the angular distributions are isotropic. We obtain the integral cross sections at $E_{\text{cm}} = 3.112$, 4.312, 6.812, 9.312 MeV, using data presented in Fig. 8 and Table 1 from Ref. [20]. As a first step we find the coefficients A_0, and then these coefficients are multiplied by 4π. The calculated integral cross sections for the two cases from Table 1 of Ref. [20] agree within their respective margins of error. These results are shown in Fig. 1, which lie somewhat lower than the data given in [8] for capture to the GS, but higher than the results reported in Ref. [6], where the sum of the cross sections for transitions to the GS and FES of ^{5}Li were measured.

Using the polarized deuteron beam with $E_{cm} = 0.48$ MeV, a thick target of ^{3}He, which completely absorbed the beam energy, the angular distribution of the products of the reaction of deuteron capture by the ^{3}He to the ground state of ^{5}Li was measured in Ref. [10]. The obtained angular distribution of γ quanta was isotropic within the error of 10%. In a similar work [9] were presented data for a polarized deuteron beam with $E_{lab} = 0.6$ MeV and a ^{3}He target in which the deuterons lost 0.3 MeV. Within the experimental error, the differential cross sections reported in Refs. [9] and [10] coincide. The total cross section, obtained from these differential cross sections is 23 μb and depicted in Fig. 1 in position of the first resonance of the reaction, i.e. at $E_R = E_{cm} = 0.27$ MeV.

To conclude this review we note that the aforementioned difference in the energy of the channel reported by [18] and [19] force us to recalculate this energy. We used data for the masses of ^{2}H and ^{3}He 1875.613 MeV and 2808.392 MeV, respectively, from [21], and the mass of ^{5}Li (4667.617 MeV) was taken from the database of [22]. Then, for the binding energy of the ^{3}He^{2}H channel of ^{5}Li, a value of 16.388 MeV is obtained, which, within precision of rounding errors, coincides with 16.39 MeV given in Ref. [19]. As we have already mentioned, a value of 16.66 MeV presented in [18] differs significantly from our results and the data of the survey of [19]. For ^{5}He in the ^{3}H^{2}H channel with $m(^3\text{H}) = 2808.921$ MeV [21] and $m(^5\text{He}) = 4667.838$ MeV [22], we have obtained the binding energy $E = 16.696$ MeV, which is in good agreement with 16.70 MeV reported in Ref. [19]. At the same time, the value of 16.792 MeV given by Tilley et al. (2002) also differs noticeably from our results and the data of [19].

2.3. Application to plasma

Now let us consider other experimental studies related to the plasma of synthesis reactors performed in Refs. [17,23,24], which are applicable when considering the plasma of synthesis reactors. Ref. [17] presented an astrophysical S-factor at zero energy and the total cross section of the ^{2}H(^{3}He, γ)^{5}Li reaction for the capture to the GS at 40 keV in c.m. In Ref. [23], the reaction rate of the ^{2}H(^{3}He, γ)^{5}Li capture to the GS is given and we use the latter rate further to compare with our results. The results for the total cross sections and the astrophysical S-factor for the capture to the GS at the energy range 13–120 keV in c.m are given and the reaction rate at temperatures up to 1.0 T_9 is presented in Ref. [11]. These results are also obtained for their application and use in the study of thermonuclear processes in the plasma of artificial thermonuclear fusion reactors. In Fig. 1 the corresponding integral cross sections from Ref. [11] for nuclei not screened by the electron shells of atoms are depicted by the solid curve.

All these results are based on the experimental work of [24], in which the ^{3}He(^{2}H, γ)^{5}Li reaction was studied at $E_{cm} = 0.025$–0.06 MeV. In Ref. [24] the branching ratios for the ^{3}He(^{2}H, γ_0)^{5}Li/^{3}He(^{2}H, p)^{4}He at five energies within the aforementioned range and for the ^{3}He(^{2}H, γ_1)^{5}Li/ ^{3}He(^{2}H, p)^{4}He at $E_{cm} \approx 0.06$ MeV were measured within the errors range 12% to 40%. It is shown In Ref. [24], that the ratio of the branching of ^{3}He(^{2}H, γ_0)^{5}Li/ ^{3}He(^{2}H, p)^{4}He in the range of $E_{cm} = 0.025$–0.06 MeV is practically constant and equal to $(4.5 \pm 1.2) \cdot 10^{-5}$, and for the case of ^{3}He(^{2}H, γ_1)^{5}Li/ ^{3}He(^{2}H, p)^{4}He at $E_{cm} \approx 0.06$ MeV the value of $(8 \pm 3) \cdot 10^{-5}$ is obtained. Moreover, the authors of Ref. [24] were carried out a simple extrapolation of the branching ratio for the ^{3}He(^{2}H, γ_0)^{5}Li/ ^{3}He(^{2}H, p)^{4}He to the point of 0 keV and the value of $(8 \pm 2) \cdot 10^{-5}$ was obtained. However, it is possible that the increased value of the branching ratio for the transition to the ground state obtained at the lowest energy in Ref. [24] can be explained by the large error of about 40%, and that in fact the ratio of the branching for the ^{3}He(^{2}H, γ_0)^{5}Li/^{3}He(^{2}H, p)^{4}He is constant up to 0 keV and equal to $(4.5 \pm 1.2) \cdot 10^{-5}$.

To obtain the integral cross sections of the reaction ^{3}He(^{2}H, $\gamma_{0,1}$)^{5}Li in the energy region $E_{\rm cm} = 0.025$–0.06 MeV, presented in Fig. 1, we use data from Refs. [24] and [25] given in Fig. 4 and Table 1 respectively. Ref. [25] presents the astrophysical S-factor of the ^{3}He(^{2}H, p)^{4}He reaction for $E_{\rm cm} = 0.008$–0.06 MeV with an error of about 3%. First, from the S-factors given in [25] we obtain the integral cross sections for the energies considered in Ref. [24], and then these cross sections we multiply by the values of the branching ratios for the ^{3}He(^{2}H, $\gamma_{0,1}$)^{5}Li/^{3}He(^{2}H, p)^{4}He from [24]. Moreover, it can be seen from Fig. 4 in Ref. [25] that in the range of $E_{\rm cm} = 0.025$–0.06 MeV, the S-factors of the ^{3}He(^{2}H, p)^{4}He reaction for screened by the electron shells of the target atoms nuclei differ from S-factors for bare nuclei by no more than 5%. Therefore, in constructing the experimental bare integrated cross sections for the ^{3}He(^{2}H, $\gamma_{0,1}$)^{5}Li reactions with an accuracy of 13–41%, we do not take into account the screening effects.

2.4. Some theoretical results

There are theoretical studies [26–29], which provide based on various approaches descriptions of either the differential cross sections and the polarization characteristics, or the spectral levels and their widths. Modern "*ab initio*" microscopic calculations for systems with $A = 5$, as well as the reactions ^{3}H(^{2}H, n)^{4}He and ^{3}He(^{2}H, p)^{4}H in the context of applications to thermonuclear processes in the Big Bang and laboratory fusion are presented in Ref. [30]. However, the processes of radiation capture, for example, ^{3}He(^{2}H, γ)^{5}Li the authors did not consider. Theoretical calculations that would include the main static and dynamic characteristics of the reaction ^{3}He(^{2}H, γ)^{5}Li and the final nucleus ^{5}Li could not be found, at least in the sources available to us. As a result one can conclude that consideration of all the experimental and theoretical works presented above, the capture reaction ^{3}He(^{2}H, γ)^{5}Li does not seem to be sufficiently studied both in the experimental and theoretical senses.

Below our expertise and a lot of experience in using the single-channel modified potential cluster model (MPCM) with forbidden states (FS) and the classification of cluster states according to Young diagrams [31–39], are applied to study the radiative ^{3}He(^{2}H, γ)^{5}Li capture. This model is much simpler than the known Resonating Group Method (RGM) [40] and its modifications [41,42], but in many cases it allows one to obtain quite reliable numerical results for many reactions such as radiative capture. In particular, on the basis of a unified concept and calculation methods, MPCM allowed one to describe the main characteristics of already 30 thermonuclear processes of radiative capture at astrophysical and thermal energies [31,32].

3. Model and some theoretical methods

The modified potential cluster model, which is used in the present calculations, is described in detail in Refs. [31,32] and, in part, in Refs. [33–39]. One of its modifications relies on the explicit dependence of the interaction potentials on Young orbital diagrams and on taking into account the mixing of cluster states according to these diagrams. The explicit dependence of the potentials on Young diagrams was taken into account already in Ref. [43]. As a result, the wave functions (WF) of the relative motion of clusters can be mixed by orbital diagrams [32,35,36,43, 44]. A similar situation was observed earlier, for example, in the n^2H [35,43], p^3H [36,44] or ^{2}H^{3}He(^{2}H^{3}H) systems [43], affecting the interaction potentials, which are used in calculations, for example, of the radiative capture total cross sections.

3.1. General definitions

All general expressions for the calculation of various nuclear characteristics which we are using in the present work are given in our early papers [31,32,45,46]. In particular, following Refs. [31,32] the expressions for the total cross sections can be written as

$$\sigma_c(NJ, J_f) = \frac{8\pi K e^2}{\hbar^2 q^3} \frac{\mu}{(2S_1+1)(2S_2+1)} \frac{J+1}{J[(2J+1)!!]^2} A_J^2(NJ, K) \cdot \sum_{L_i, J_i} P_J^2(NJ, J_f, J_i) I_J^2(J_f, J_i). \tag{1}$$

In Eq. (1) μ is reduced mass in the initial channel, q is the wave number in fm^{-1} related to the c.m. energy as $q^2 = (2\mu E)/\hbar^2$, S_1 and S_2 particle spins in the initial channel, K and J are the wave number and the momentum of the emitted γ quantum, and N denotes electric E or magnetic M transitions of rank J from the initial J_i to the final J_f states. For electric convection $EJ(L)$ transitions ($S_i = S_f = S$) there are the following expressions for P_J, A_J and I_J in Eq. (1) [31,32]:

$$P_J^2(EJ, J_f, J_i) = \delta_{S_i S_f}\big[(2J+1)(2L_i+1)(2J_i+1)(2J_f+1)\big](L_i 0 J 0 | L_f 0)^2 \begin{Bmatrix} L_i & S & J_i \\ J_f & J & L_f \end{Bmatrix}^2,$$

$$A_J(EJ, K) = K^J \mu^J \left(\frac{Z_1}{m_1^J} + (-1)^J \frac{Z_2}{m_2^J} \right), \qquad I_J(J_f, J_i) = \langle \chi_f | r^J | \chi_i \rangle. \tag{2}$$

Here S_i, S_f, L_f, L_i, J_f, J_i are the corresponding momenta in the initial and final states, m_1, m_2, Z_1, Z_2 are masses and charges in the initial channel, and I_J is the overlapping integral over the radial functions for the scattering χ_i and bound χ_f states, depending on the cluster-cluster relative coordinate r.

For the spin dipole magnetic $M1(S)$ transition, i.e. for $J = 1$, the following expressions were obtained ($S_i = S_f = S$, $L_i = L_f = L$) [31,32]

$$P_1^2(M1, J_f, J_i) = \delta_{S_i S_f} \delta_{L_i L_f} \big[S(S+1)(2S+1)(2J_i+1)(2J_f+1)\big] \begin{Bmatrix} S & L & J_i \\ J_f & 1 & S \end{Bmatrix}^2,$$

$$A_1(M1, K) = i \frac{\hbar K}{m_0 c} \sqrt{3} \left(\mu_1 \frac{m_2}{m} - \mu_2 \frac{m_1}{m} \right), \quad I_J(J_f, J_i) = \langle \chi_f | r^{J-1} | \chi_i \rangle. \tag{3}$$

In Eq. (3) $m = m_1 + m_2$ is the mass of nucleus, μ_1, μ_2 are the magnetic moments of the clusters [47], all other notations are the same as in Eq. (2). For the light clusters $\mu(^2\mathrm{H}) = 0.857438$, $\mu(^3\mathrm{H}) = 2.978662$, $\mu(^3\mathrm{He}) = -2.127625$. The exact values for the particle masses use: $m(^2\mathrm{H}) = 2.013553$ amu, $m(^3\mathrm{H}) = 3.015501$ amu, and $m(^3\mathrm{He}) = 3.014932$ amu [21]. The constant $\hbar^2/m_0$ is equal to 41.4686 MeV fm^2, where m_0 is the atomic mass unit (amu). The Coulomb parameter $\eta = (\mu Z_1 Z_2 e^2)/(\hbar^2 q) = 3.44476 \cdot 10^{-2} (\mu Z_1 Z_2)/q$. The Coulomb potential for the point-like particles is of the form $V_c(\mathrm{MeV}) = 1.439975(Z_1 Z_2)/r$. Here we are giving the numerical values as the accuracy of the further calculations depends strongly over them, especially in the resonance energy ranges, as well as the ^{5}Li binding energy in ^{2}H^{3}He cluster channel. Principles for constructing intercluster potentials, numerical calculation methods and some computer programs on FORTRAN-90 are given in Refs. [31,32] and partly in Refs. [33,35].

Table 2
Classifications of the allowed (AS) and forbidden states (FS) in cluster systems with $A = 5$. Here T, S and L are isospin, spin and the orbital angular momentum of the particle system, $\{f\}_S$, $\{f\}_T$, $\{f\}_{ST}$ and $\{f\}_L$ are spin, isospin, spin-isospin, and possible orbital Young diagrams, respectively and $\{f\}_{AS}$, $\{f\}_{FS}$ are Young diagrams of allowed and forbidden orbital states.

System	T	S	$\{f\}_S$	$\{f\}_T$	$\{f\}_{ST}$	$\{f\}_L$	L	$\{f\}_{AS}$	$\{f\}_{FS}$
$^2H^3He$ $^2H^3H$	1/2	1/2	{32}	{32}	{5} + {41} + {32} + {311} + + {221} + {2111}	{5}	0	–	{5}
						{41}	1	{41}	–
						{32}	0,2	{32}	–
		3/2	{41}	{32}	{41} + {32} + {311} + {221}	{5}	0	–	{5}
						{41}	1	–	{41}
						{32}	0,2	{32}	–

3.2. Potentials for elastic $^2H^3He$ scattering

We present the classification by orbital symmetries of the $^2H^3He$ and $^2H^3H$ systems, i.e. a configuration of $2 + 3$ nucleons. The doublet channel spin ($S = 1/2$) scattering states depend on the two allowed orbital Young diagrams {41} and {32}, and these are regarded as mixed in terms of the orbital symmetries. The quartet channel spin ($S = 3/2$) allows only one symmetry {32}, so these states are pure according to the Young diagrams. Therefore, it is assumed that states with a minimal spin in some lightest cluster systems scattering processes, including those considered here, can turn out to be mixed in Young orbital diagrams, as was shown in [43] and some previous works of these authors (see references in [43]).

The classification of states according to Young diagrams for these systems is given in Table 2 and was obtained in [43,45] on the basis of general tables of Young diagrams products from [48]. Table 2 shows the forbidden state with the Young diagram {5} for the S-waves of doublet and quartet channels, while in the P-wave the forbidden state with the Young diagram {41} is present only for the quartet channel, in the doublet channel this state is allowed.

At the same time, the states of clusters in the discrete spectrum, for example, the ground states of ^{5}He and ^{5}Li nuclei are assumed to be pure with the Young diagram {41} [43]. Furthermore, it is assumed that since the scattering states and the discrete spectrum depend on different Young diagrams, it is possible to juxtapose them different interaction potentials. In other words, explicit dependence of the potentials on the orbital symmetries $\{f\}$ is allowed, and not only on the quantum numbers *JLS* – total angular momentum, orbital angular momentum and spin of the nuclear particles system [43]. In more detail, the case with the mixing of cluster states by Young diagrams was described by us in recent publications [35,36].

We note that the total angular momentum $J = 3/2^-$ for the GS or $J = 1/2^-$ for the FES in P waves of ^{5}He or ^{5}Li nuclei can also be obtained in the doublet spin channel of $^2H^3He$ ($^2H^3H$) clusters with total spin $S = 1/2$ and in the quartet channel with $S = 3/2$. Therefore, the GS and FES of these systems are actually ^{2+4}P mixtures of such channels. These spin-mixed ^{2+4}P states turn out to be mixed also according to Young diagrams, since the doublet pure channel corresponds to the {41} diagram, and the quartet channel to the {32} one. However, now only one Young diagram corresponds to each spin channel, but not two, as it was in the previous case with mixing one spin channel in terms of orbital symmetries. Therefore, the potentials obtained below with $J = 3/2^-$ and $1/2^-$ for GS and FES are called pure, although in reality they are mixed along the spin, and, hence, along the Young diagrams.

Table 3
Parameters of the partial potentials of elastic ^{2}H^{3}He scattering. The boldfaced type indicates the potentials of the resonance states. Angular momentum and parity J^π are taken from [18,19].

$^{2S+1}L_J$	V_0, MeV	α, fm^{-2}	The resonance energy E_{cm}, MeV	The angular momentum and parity J^π
$^2S_{1/2}$, $^{2+4}D_{3/2}$	−30.0	0.15	–	
$^{2+4}D_{5/2}$	**−31.29**	**0.09**	**3.35**	**5/2$^+$**
$^2P_{1/2}$	−48.0	0.1	–	–
$^{2+4}P_{3/2}$	**−2412.2**	**4.0**	**2.89**	**3/2$^-$**
$^4S_{3/2}$	**−34.5 *(−34.85)***	**0.1**	**0.48**	**3/2$^+$**
$^4D_{1/2}$	**−39.88**	**0.115**	**4.14**	**1/2$^+$**
$^4D_{7/2}$	**31.99**	**0.09**	**3.06**	**7/2$^+$**
$^4P_{1/2}$	−30.0	0.1	–	–
$^4P_{5/2}$	**−456.7**	**0.8**	**5.67**	**5/2$^-$**

In the present calculations of the nuclear characteristics of the reaction under consideration, the interaction potentials of particles have the form of a Gaussian attraction that widely used in our previous works

$$V(r, JLS\{f\}) = V_{0,JLS\{f\}} \exp(-\alpha_{JLS\{f\}} r^2) + V_c(r) \tag{4}$$

with the Coulomb potential $V_c(r)$ of two point particles for the zero Coulomb radius that has the form which was given above.

Follow Ref. [49] we considered the ^{2}H^{3}He scattering phase shifts in the energy range up to 3 MeV in the c.m., which are sufficient for solving various astrophysical problems, in particular, for calculating the total cross sections for the capture reaction. Parameters of partial, i.e. depending on $^{2S+1}L_J$, potentials of the continuous spectrum, given in Table 3, including the resonance states potentials, which are described in detail below. The characteristics of these states are given in the last column of Table 3.

The phase shifts of the *non-resonance doublet potentials* from Table 3, given in ordinary type, are shown by the solid curves in Fig. 2a. For the potential of the $^2D_{3/2}$ wave the parameters of the $^2S_{1/2}$ potential at $L = 2$ were used. In $P_{3/2}$ and $D_{5/2}$ scattering waves that are mixed along the spin channel, there are resonances that follow from the nuclear spectra shown in Table 1 [18,19]. Parameters of such potentials are given in bold face in Table 3 and the corresponding phase shifts are shown in Fig. 2a by the dashed curves.

Let us further consider the potentials for quartet scattering states whose phase shifts are shown by the solid curves in Fig. 2b. If we plot the $^4S_{3/2}$ potential over the scattering phase shifts, the parameters from Table 3 can be used. The phase shift of this potential is shown in Fig. 2b by the solid curve 1. Using this potential at $L = 2$ the $^4D_{3/2}$ phase shift is obtained. It is shown in Fig. 2b by the solid curve 2. At 3.7 MeV in the c.m. the potential leads to a resonance with a width of 4.3 MeV in the c.m. It should be noted that in the spectra shown in Table 1 such a resonance is not observed. Therefore, for $^4D_{3/2}$ waves we will use the $^2D_{3/2}$ scattering potential, since these states are spin-mixed with the same total momentum.

Now we recall that we use a single-channel $d + ^3$He model in which the influence of other channels is not taken into account. To substantiate the using of a single-channel model in this case, we provide interesting results from [30], where they considered $d + ^3$He elastic scattering in the framework of the *ab initio* method. In Fig. 2c we compare our theoretical calculations of the doublet and quartet S scattering phase shifts performed within the framework of the MPCM

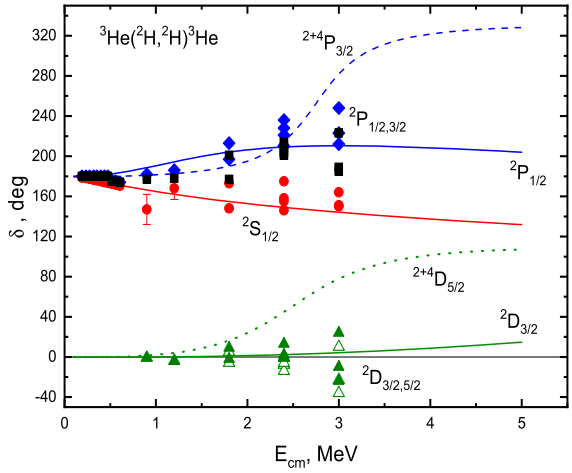

Fig. 2a. Comparison of the ^{2}H + ^{3}He doublet phase shifts (solid curve) mixed by orbital diagrams calculated using the potential (4) and the parameters from Table 3 with results from [49]. Black squares (■) and rhombuses (◆) – results from [49] for the $^2P_{1/2}$ and $^2P_{3/2}$ waves, triangles – for the $^2D_{3/2}$ (Δ) and $^2D_{5/2}$ (▲) waves, dots (●) – for the $^2S_{1/2}$ wave. The notation for several total momentums $^2P_{1/2,3/2}$ refers to the results of [49]. The preliminary results of these calculations were reported in [50].

with to *ab initio* calculations [30] and the experimental data. From the figure one can see that for the $^2S_{1/2}$ phase shift all variations of the calculations for a different number of channels yield very close results, i.e. the influence of other channels is almost negligible. For the *ab initio* $^4S_{3/2}$ phase shift channel coupling accounting (dashed and dotted curves) also appears very slightly.

The real agreement of the scattering phase shifts extracted from the experiment [49], the present calculations, and *ab initio* is observed only when the channel p + ^{4}He and channel ^{2}H* + ^{3}He with the excited deuteron coupling is used in [30]. In our opinion, this is a rather unexpected result, which, apparently, requires physical substantiation and interpretation. At the same time, for the purposes of our work, we can assume that the presented comparison makes it possible to draw a conclusion that the single-channel approximation employed in the present work is justified, since taking into account the two channels p + ^{4}He and ^{2}H* + ^{3}He in the *ab initio* method practically does not change the results for the scattering phase shifts in the single-channel case. It is well know that at low energies the asymptotic part of wave function plays a significant role in the most of nuclear processes, but at high energy the internal part of the wave function is very important due the strong NN interaction at small distances, while the latter one has a slight influence on low energy characteristics of reactions.

Let us now consider in more detail the potentials for partial waves with resonances. Table 1 clearly shows the first resonance of ^{5}Li, which is 0.482 MeV above the ^{2}H^{3}He channel threshold. The excitation energy, momentum and width in c.m. are 16.87 MeV, $J^\pi = 3/2^+$, 0.267 MeV, respectively. This state can be attributed to a $^4S_{3/2}$ wave of the continuous spectrum, and its description requires a potential with FS for the diagram {5} and parameters

$$V_{S3/2} = -34.85 \text{ MeV} \quad \text{and} \quad \alpha = 0.1 \text{ fm}^{-2} \tag{5}$$

which lead to a resonance energy of 0.480(1) MeV in c.m. The corresponding phase shift is shown in Fig. 2b with the red dashed curve 1. For $L = 2$, the potential gives a ^{4}D$_{3/2}$ phase shift resonance at 3.6(1) MeV in c.m. with a width of 4.1(1) MeV in c.m. Its phase shift is shown

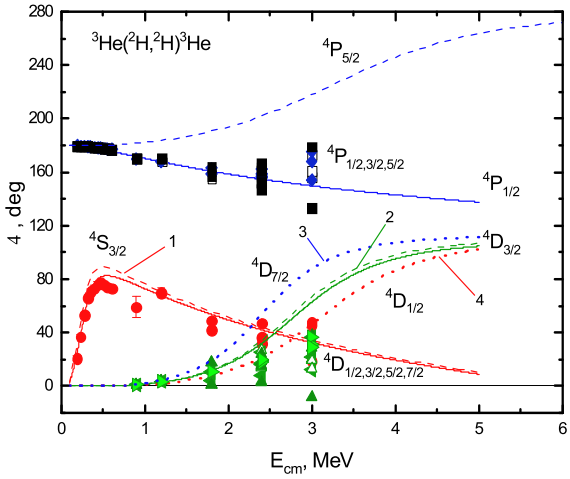

Fig. 2b. Comparison of the ^{2}H + ^{3}He quartet phase shifts (solid curves), which pure by orbital diagrams calculated using the potential (4) and the parameters from Table 3 with results from [49]. Black squares (■), rhombuses (◆) and blank squares (□) – results from [49] for the $^4P_{1/2}$, $^4P_{3/2}$ and $^4P_{5/2}$ waves, triangles – for the $^4D_{1/2}$ (▲), $^4D_{3/2}$ (△), $^4D_{5/2}$ (◄) and $^4D_{7/2}$ (►) waves, dots – for the $^4S_{3/2}$ wave. The notation for several total momentums $^4P_{1/2,3/2,5/2}$ is explained in Fig. 2a. (For interpretation of the colors in the figure(s), the reader is referred to the web version of this article.)

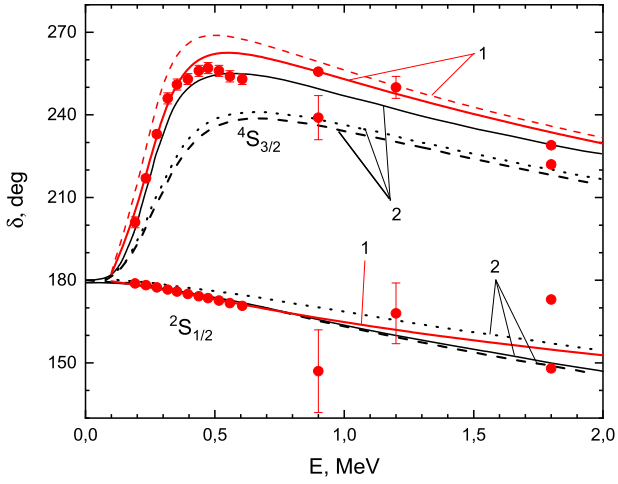

Fig. 2c. Comparison of the calculations of the scattering S phase shifts for potentials in MPCM (group 1, red curves) and in *ab initio* [30] (group 2, black curves). The dashed curve – calculation taking into account the coupling of the $p + {}^4$He and $d + {}^3$He channels; dotted curve – calculation ***without regard*** to channel coupling; solid curve – calculation taking into account the channel $p + {}^4$He and the excited deuteron in the $d^* + {}^3$He channel coupling.

in Fig. 2b with the dashed curve 2. The potential with parameters (5) differs little from the one given in Table 3, but more accurately describes the resonance energy. At the resonance energy of 0.480 MeV, it leads to the scattering phase shift equal to 89.45°.

The second resonance in the ^{2}H^{3}He system appears at 19.28 MeV with the angular momentum $J^\pi = 3/2^-$ and width of 0.959 MeV [18] is laying at 19.28 MeV relative to the GS (2.892 MeV

towards the channel threshold). The $P_{3/2}$ wave may match this state in doublet or quartet spin channel. The phase shift analysis presented in [49] shows no any resonance behavior of the $P_{3/2}$ waves. While, the ^2P phase shift illuminates the smooth rising in the doublet channel, its quartet partner ^4P is clearly slowly decreasing. For properly reproducing this $^{2+4}P_{3/2}$ resonance we need a potential with the FS and the following parameters:

$$V_{\mathrm{P3/2}} = -2412.2 \text{ MeV} \quad \text{and} \quad \alpha = 4.0 \text{ fm}^{-2}. \tag{6}$$

The potential (6) provides the following resonance parameters: the position is fitted at the energy of 2.890(1) MeV in the c.m., and the corresponding width is 0.962(1) MeV in c.m. Its $P_{3/2}$ phase shift is shown in Fig. 2a with a dashed curve, and at the resonance energy it has a value of 90.0(1)°.

In Table 1 the second column shows the higher laying levels for $J^\pi = 7/2^+$ and $J^\pi = 5/2^+$ with the following corresponding parameters: the energy position of 19.45 and 19.71 MeV relative to the GS (or 3.06 and 3.32 MeV in c.m. relative to the channel threshold), the level width of 3.28 and 4.31 MeV in c.m. (see Table 5.3 in [18]). The strong $E1$ transitions to the GS are conditioned by direct capture from the doublet and quartet channels corresponding to the second $5/2^+$ resonance. For a correct description of the $^{2+4}D_{5/2}$ resonance a potential without the FS and with the following parameters

$$V_{\mathrm{D5/2}} = -31.29 \text{ MeV} \quad \text{and} \quad \alpha = 0.09 \text{ fm}^{-2} \tag{7}$$

is needed.

The calculated $D_{5/2}$ scattering phase shift is shown in Fig. 2a with the dotted curve. At the resonance energy the value of this phase shift is 90.0(1)°. The calculated resonance parameters are the following: the energy position of 3.32(1) MeV in c.m., and the width of 4.09(1) MeV in c.m. There is no resonance for the $D_{5/2}$ phases shift at such energies in Ref. [49]. The ^4D phase shifts have a slight tendency to rise at 3.0 MeV in c.m. Let us mention that some our preliminary results [50] of these calculations are different than results of the calculations shown in Fig. 2a.

The level with $J^\pi = 7/2^+$ at 3.06 MeV in c.m. and a width of 3.28 MeV in c.m. can be attributed to the $^4D_{7/2}$ state. In this case the $M2$ transition to the GS is possible, the total cross sections for which will be noticeably smaller than the cross sections for the $E1$ processes. However, we give the potential without the FS for this resonance the following parameters

$$V_{\mathrm{D7/2}} = -31.99 \text{ MeV} \quad \text{and} \quad \alpha = 0.09 \text{ fm}^{-2}. \tag{8}$$

This potential leads to the resonance at the energy of 3.06(1) MeV in c.m. with a width of 3.18(1) MeV in c.m., and its $D_{7/2}$ scattering phase shift is shown in Fig. 2b with the dotted curve 3. At the resonance energy the phase shift has a value of 90.0(1)°.

The next level can be detected at the excitation energy of 20.53 MeV or at 4.14 MeV in c.m. with a momentum $J^\pi = 1/2^+$ and a width of 5.0 MeV in c.m., so it can be attributed to the $^4D_{1/2}$ resonance. A correct description of such resonance requires a potential with the following parameters:

$$V_{\mathrm{D1/2}} = -39.88 \text{ MeV} \quad \text{and} \quad \alpha = 0.115 \text{ fm}^{-2} \tag{9}$$

This potential leads to the resonance at the energy of 4.14(1) MeV in c.m. with a width of 5.1(1) MeV in c.m., and its scattering phase shift is shown in Fig. 2b by the dotted curve 4. At resonance energy the phase shift has a value of 90.0(1)°.

Table 4
Updated potential parameters for the ^{2}H^{3}He system in pure state by Young diagrams for the GS and FES. Here the width parameter α is equal to 0.18 fm^{-2}. The binding energy of the FES is taken from [18], where 1.49 MeV above the GS is given.

L_J	V_0, MeV	E_{bs} (E_{exp} ([18]), MeV	C_w	R_{rms}, fm
$P_{3/2}$ (GS)	−83.505593	−16.388000 (−16.388)	6.30(1)	2.25
$P_{1/2}$ (FES)	−80.485333	−14.898000 (−14.898)	5.74(1)	2.26

Let us consider one more level, which lies at an excitation energy of 22.06 MeV or 5.67 MeV in c.m. with a momentum $J^\pi = 5/2^-$ and a width of 15.5 MeV in c.m. This resonance can be attributed to the $^4P_{5/2}$ state. A potential with the FS and parameters

$$V_{\text{P5/2}} = -456.7 \text{ MeV} \quad \text{and} \quad \alpha = 0.8 \text{ fm}^{-2} \tag{10}$$

is required to correctly describe the $^4P_{5/2}$ state.

The potential leads to the resonance at the energy of 5.67(1) MeV in c.m. with a width of 15.7(1) MeV in c.m., and its scattering phase shift is shown in Fig. 2b with a dotted curve 3; at the resonance energy the phase shift has a value of 90.0(1)°.

The detailed study of these levels shows that the phase shift analysis performed in Ref. [49] does not take into account the position of the resonances under consideration with large widths. The phase shift analysis is a subject to further refinement with the expansion of the energy region to 5–7 MeV in c.m. However, in order to make a detailed phase shift analysis the measurements of differential cross sections in the energy region of interest in steps of 0.3–0.5 MeV (in the region of narrow resonances the energy step should be even smaller) is required. In order to properly depict the phase shift resonance, it is required to have a step of measuring cross sections in the resonance region of not less than Γ/5. In other words, within the width of the resonance there must be at least five points of the cross sections measurement. Only in this case the resonance form of the phase shift appears quite accurately [51]. For example, for a resonance of the potential (6) described with a width of about $\Gamma \sim 1$ MeV, a step of ∼0.2 MeV is needed. For the potential (5) with resonance in the ^4S wave, the energy step should be of the order of 0.05–0.06 MeV.

3.3. *Potentials for $^2H^3He$ bound states*

Now consider the potential of the GS of ^{5}Li in the ^{2}H^{3}He channel. The P states with potentials from Table 3 allowed in the doublet and quartet channels have an energy that does not agree with the binding energy of the $P_{3/2}$ and $P_{1/2}$ levels of the ground and first excited states of ^{5}Li, whose spectrum is shown in Table 1. These potentials depend on two Young orbital diagrams, and the BS potential should depend only on one orbital diagram {41} [43]. In addition, the channel energies for the GS and FES of ^{5}Li were specified above. Therefore, we carried out a refinement of the potentials of these BSs and the results are given in Table 4. In the calculations of the BS energy the exact masses of the particles were used, and the relative accuracy of the calculations for binding energy is at a level of 10^{-6} MeV [35].

In Table 4, in the third column, the experimental energy values of the levels [18] are given in parenthesis. The dimensionless asymptotic normalizing coefficients (ANC) C_w are given in the last column in Table 4. They are defined according to Ref. [52]

$$\chi_L(R) = \sqrt{2k_0} C_w W_{-\eta L+1/2}(2k_0 R). \tag{11}$$

Table 5
Transitions accounted for calculations the total radiative ^{3}He(^{2}H, γ)^{5}Li capture cross section.

No.	$(2S+1L_J)_i$	The resonance energy in MeV	The angular momentum and parity J^π	Transition	$(^{2S+1}L_J)_f$	P^2
1.	$^2S_{1/2}$	–		$E1$	$^2P_{3/2}$	4
2.	$\boldsymbol{^4S_{3/2}}$	**16.87**	**3/2$^+$**	$\boldsymbol{E1}$	$\boldsymbol{^4P_{3/2}}$	**4**
3.	$^2P_{1/2}$	–		$M1$	$^2P_{3/2}$	4/3
4.	$\boldsymbol{^2P_{3/2}}$	**19.28**	**3/2$^-$**	$\boldsymbol{M1}$	$\boldsymbol{^2P_{3/2}}$	**5/3**
5.	$^4P_{1/2}$	–		$M1$	$^4P_{3/2}$	10/3
6.	$\boldsymbol{^4P_{3/2}}$	**19.28**	**3/2$^-$**	$\boldsymbol{M1}$	$\boldsymbol{^4P_{3/2}}$	**22/15**
7.	$\boldsymbol{^4P_{5/2}}$	**22.06**	**5/2$^-$**	$\boldsymbol{M1}$	$\boldsymbol{^4P_{3/2}}$	**18/5**
8.	$^2D_{3/2}$	–		$E1$	$^2P_{3/2}$	4/5
9.	$\boldsymbol{^2D_{5/2}}$	**19.71**	**5/2$^+$**	$\boldsymbol{E1}$	$\boldsymbol{^2P_{3/2}}$	**36/5**
10.	$\boldsymbol{^4D_{1/2}}$	**20.53**	**1/2$^+$**	$\boldsymbol{E1}$	$\boldsymbol{^4P_{3/2}}$	**2/5**
11.	$^4D_{3/2}$	–		$E1$	$^4P_{3/2}$	64/25
12.	$\boldsymbol{^4D_{5/2}}$	**19.71**	**5/2$^+$**	$\boldsymbol{E1}$	$\boldsymbol{^4P_{3/2}}$	**126/25**

In Eq. (11) $\chi_L(R)$ is the numerical GS radial WF, viz. the solution of the Schrödinger equation normalized to unit, $W_{-\eta L+1/2}(2k_0R)$ is Whittaker function, k_0 is a wave number related to the channel binding energy, η is the Coulomb parameter, L is the orbital angular momentum of the bound state [31]. The pointed ANC error is determined by its averaging over the interval from 5–6 up to 8–10 fm and shown in parenthesis. The charge root mean square radii (R_{rms}) for the BSs of ^{5}Li in the ^{2}H^{3}He channel were also calculated and are given in Table 4.

Since the ground $P_{3/2}$ state is spin-mixed, it is necessary to consider the $E1$ transitions from the doublet and quartet states of S and D scattering. In the framework of the model under consideration, it is impossible to explicitly isolate the $^2P_{3/2}$ and $^4P_{3/2}$ parts in the WF of the GS. So, for the calculations we will use the spin-mixed function of the $P_{3/2}$ state, which is obtained when solving the Schrödinger equation with a given GS potential from Table 4. For the scattering states quartet and mixed over the Young diagrams doublet potentials from Table 3 are used and also the resonance potentials (5)–(10).

3.4. Multipole transitions

The complete set of $E1$ and $M1$ transition amplitudes accounted in our calculations is given in Table 5. Transitions from the resonance state with the main input to the total cross sections are marked as bold. Transitions from non-resonance scattering states give a noticeably smaller contribution at low energies. The last column contains the values of the coefficient P^2 in expressions (2) and (3).

The interaction potentials have been corroborated by the experimental data on the elastic scattering phase shifts and energy levels spectra, so, the WFs obtained as the solutions of the Schrödinger equation with those potentials account effectively the cluster system states, in particular, of the mixing by channel spin. Therefore, the total cross section of the $E1$ transition from the mixed continuous states to the spin mixed GS may be taken as simple doubling of the partial cross section as each is calculated with the same functions. However, spin algebraic factors are specified for every matrix element (2) [31,32]:

$$\sigma_0(E1) = {}^2\sigma\left({}^2D_{3/2} \to {}^2P_{3/2}\right) + {}^4\sigma\left({}^4D_{3/2} \to {}^4P_{3/2}\right).$$

In reality, there is only one transition from the scattering state to the GS, rather than two different $E1(^2\sigma + {}^4\sigma)$ processes. The averaging procedure concerns the transitions from the $D_{5/2}$ and $D_{3/2}$ scattering states to the $P_{3/2}$ GS of ^{5}Li in the ^{2}H^{3}He channel. This approach, which we proposed earlier for transitions in neutron radiative capture on ^{15}N [32], was used for some other reactions, and allowed us to obtain reasonable results in describing the total cross sections [32].

Thus, the total cross section of the capture process on the GS for electromagnetic $E1$ transitions is represented as the following combination of partial cross sections

$$\begin{aligned}\sigma_0(E1) = {} & \sigma\left({}^2S_{1/2} \to {}^2P_{3/2}\right) + \sigma\left({}^4S_{3/2} \to {}^4P_{3/2}\right) + \sigma\left({}^4D_{1/2} \to {}^4P_{3/2}\right) \\ & + \left[\sigma\left({}^2D_{3/2} \to {}^2P_{3/2}\right) + \sigma\left({}^4D_{3/2} \to {}^4P_{3/2}\right)\right]/2 \\ & + \left[\sigma\left({}^2D_{5/2} \to {}^2P_{3/2}\right) + \sigma\left({}^4D_{5/2} \to {}^4P_{3/2}\right)\right]/2.\end{aligned}$$

Since for the $M1$ transitions there is also spin mixing for some Pscattering waves, the total cross section is written in the same way as $E1$ transitions to the GS:

$$\begin{aligned}\sigma_0(M1) = {} & \sigma\left({}^4P_{5/2} \to {}^4P_{3/2}\right) + \left[\sigma\left({}^2P_{1/2} \to {}^2P_{3/2}\right) + \sigma\left({}^4P_{1/2} \to {}^4P_{3/2}\right)\right]/2 \\ & + \left[\sigma\left({}^2P_{3/2} \to {}^2P_{3/2}\right) + \sigma\left({}^4P_{3/2} \to {}^4P_{3/2}\right)\right]/2.\end{aligned}$$

It should be noted that $M1$ transitions from non-resonance P scattering states exert a noticeable effect on the total cross sections only at energies above 300–400 keV in c.m. Thus, we have identified all the major transitions that may contribute to the total cross sections of the ^{3}He(^{2}H, γ)^{5}Li capture process at low energies, which are treated here. Of course, the $M2$ transition is also possible, but we do not consider it because of the smallness of its cross sections.

4. Results for total cross sections, astrophysical S-factor and reaction rate

In this Section, we present results obtained with the aforementioned potentials for the total cross section, the astrophysical S-factor, the S-factor screening effects, and the rate of the ^{3}He(^{2}H, γ)^{5}Li reaction of radiation capture.

4.1. Total cross section

The results of the calculated $E1$ and $M1$ radiative capture in ^{2}H^{3}He cluster channel at the energies up to 5.0–6.0 MeV are presented in Fig. 3. The solid curve 1 denotes the cross section for the $E1$ transition from the ^2S and ^4S scattering states to the GS $^{2+4}P_{3/2}$ defined by the interaction potential parameters from Table 4, while for the scattering potentials, the data from Table 3 are used. Cross sections for the $E1$ transitions from the ^2S wave are of few orders suppressed as it is of non-resonance behavior.

Solid curve 2 in Fig. 3 denotes the cross section for the $E1$ transition to the GS from the resonating $^{2+4}D_{5/2}$ waves calculated with parameters (7) and (9). This result includes all other small in value amplitudes for the non-resonating D waves listed in Table 3 (see Table 5). The main contribution here is given by the $D_{5/2}$ resonance, and the contribution of the $D_{1/2}$ wave is very small. Curve 3 in Fig. 3 shows the contribution of the $M1$ transitions from the resonating $^{2+4}P_{3/2}$ and $^{2+4}P_{5/2}$ waves corresponding to potentials (6) and (10) and non-resonance set for P potentials from Table 3. Fig. 3 clearly shows the $P_{3/2}$ resonance at 2.89 MeV in c.m., the value of which is even larger than the resonance for the $E1$ transition, since the additional contribution

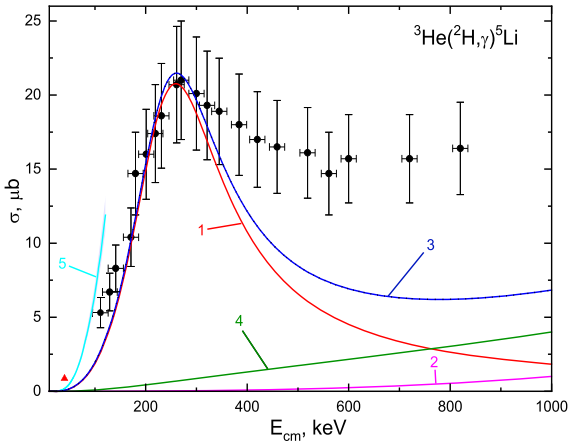

Fig. 3a. Total cross section for ^{3}He(^{2}H, γ)^{5}Li below 1.0 MeV. Experimental data from [7] – dots (●) and [17] – triangle (▲), cyan band 5 – results from [11]. Calculated curves correspond to the potential parameters from Tables 3 and 4 and text. Two last black dots are taken from Fig. 9 of the work [7].

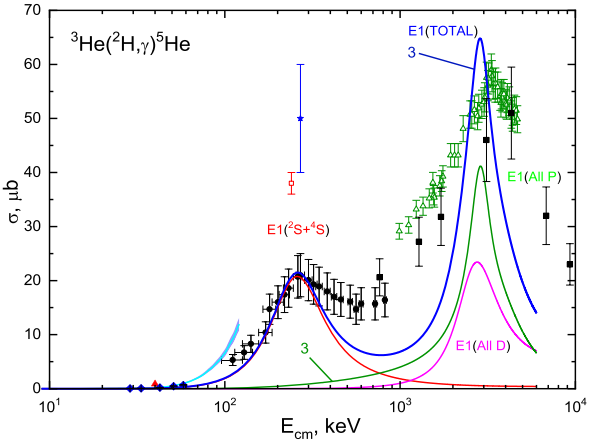

Fig. 3b. Total cross section for ^{3}He(^{2}H, γ)^{5}Li below 5.0 MeV. Experimental data from [7] – dots (●) and [17] – triangle (▲), [24,25] – rhombuses (◆), [20] – black squares (■), [8] – blank triangles (△), [4] –star (★) , [5] – blank square (□), cyan band 5 – results from [11]. Two last black dots (●) are taken from Fig. 9 of the work [7].

is given by the $P_{5/2}$ resonance. The total cross section included all $E1$ and $M1$ transitions listed above is shown by the curve 4 in Fig. 3.

In Fig. 3 one can see that at energies above 400 keV the results of our calculation are much lower than the available experimental data [7], and at energies less than 2 MeV they lie below the results obtained in [8]. This difference in the cross sections can be due to two reasons: i. in our calculations, we considered 12 different electromagnetic transitions, but perhaps some additional relevant processes were not taken into account; ii. in Refs. [7] and [8] in the energy range from 0.4 to 2 MeV the effect of capture on the FES is not entirely excluded. In addition, the maximum of the calculated cross section in the 3 MeV region is lower than the data given by Ref. [8], which can be explained by the inaccuracy of the spectra [19] known for the authors of Ref. [8],

but used by us today [18]. In both cases, the results of [7] and [8] require refinement on the basis of modern methods of experimental measurements.

We note that the experimental error of the cross sections given in Fig. 3 was taken to be 19%, as indicated by [7] for an energy of 450 keV in l.s. or 270 MeV in c.m. and the cross section 21(4) μb with an error of 15 keV for the center-of-mass energy. The data given as a function of laboratory energy in Ref. [7] were recalculated by us to the c.m. energy with integer particle masses. The data given as a function of the excitation energy in Ref. [8] were also recalculated to the c.m. energy with the binding energy of the ^{2}H^{3}He channel of 16.4 MeV, which is given by [8]. The data from [4] are given for the c.m. energy of 0.27(3) MeV, at which the maximum values of the cross sections are observed in this work. The data from [5] are given for the energy of 240 keV in the c.m. Let us note that results of calculations of the total cross section for ^{3}He(^{2}H, γ)^{5}Li presented in Fig. 3a are obtained using a renewed parametrization of the potentials in contrast to our previous calculations [50]. One can find the difference of the parameters by comparing Table 4 with the results presented in Table 3 from Ref. [50].

4.2. Astrophysical S-factor

The astrophysical S-factors that characterize the behavior of the total cross section of the nuclear reaction at an energy tending to zero are determined as follows [53]

$$S(NJ, J_f) = \sigma(NJ, J_f) E_{\text{cm}} \exp\left(\frac{31.335 Z_1 Z_2 \sqrt{\mu}}{\sqrt{E_{\text{cm}}}}\right),$$

where σ is the total cross section of the radiative capture process in barn, E_{cm} is the particle energy usually measured in keV in the center-of-mass system, μ is the reduced mass of the particles in the initial channel in amu, Z_1 and Z_2 are the charges of particles in units of elementary charge and N are the E or M transitions of the J-th multipolarity to a finite J_f state of the nucleus. The value of the numerical coefficient 31.335 is obtained on the basis of the modern values of the fundamental constants [54].

Now we present the results obtained for the astrophysical S-factor for the reaction under consideration. Fig. 4 displays the total astrophysical S-factor (the solid curve) for the transitions to the GS due to the $E1$ and $M1$ processes in direct correspondence with the cross sections shown in Fig. 3. Note, the results for the S-factor in Fig. 4 have the same qualitative behavior as our earlier reported preliminary results [50]. However, there are some variations in quantitative values. So that, S-factor at the energy of 6-30 keV in c.m. is still relatively stable but equal to 0.125(2) keV·b, which is still less comparing the experimental data reported in Ref. [7]. The error of the calculated S-factor shown here is obtained by averaging it over the indicated energy interval. The value of the calculated S-factor is 0.125 keV·b at the energy of 6 keV. At a maximum energy of 230 keV in c.m. the S-factor equals to 0.43 keV·b. If one uses for the $^4S_{3/2}$ scattering wave the resonance potential (5) obtained on the basis of the characteristics of the first resonance level, instead of its parameters from Table 3, it does not significantly change the magnitude and shape of the calculated S-factor.

We recalculated data [7] for the cross sections into S-factor and presented them as solid circles in Fig. 4. As we defined at minimal energies 100–200 keV its value is near 0.39 keV·b. This value in the indicated energy range can be approximated by a trivial constant energy dependence $S(E) = S_0$ with $S_0 = 0.386$ keV·b and a mean value for $\chi^2 = 0.21$. Experimental 19% errors were assumed for the S-factor and the result is shown by the dashed curve 1 in Fig. 4.

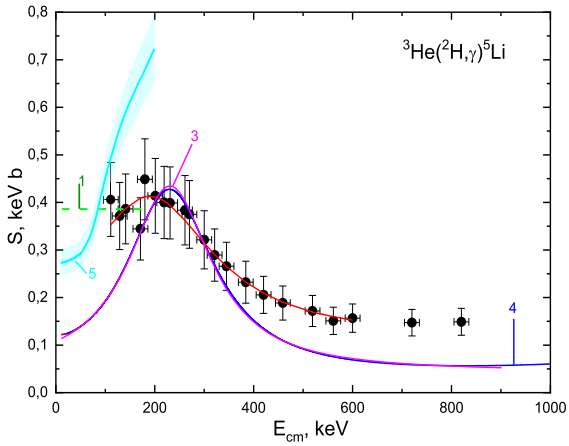

Fig. 4a. S-factor data from [7] and calculations using the potential (4) with the parameters from Tables 3 and 4 below 1.0 MeV. Data are the same as in Fig. 3a. Cyan band 5 – results from [11].

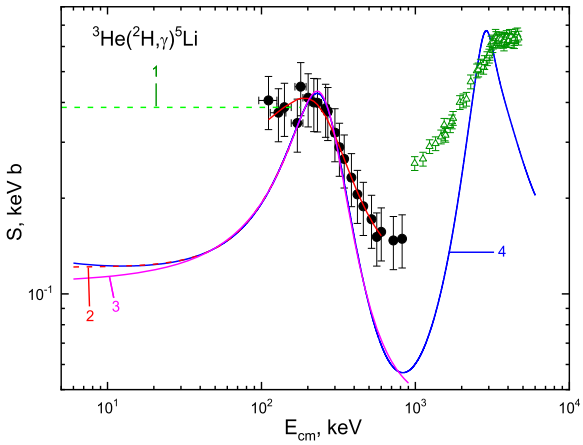

Fig. 4b. Same as in Fig. 3a, but at the energy below 5.0 MeV. Data are the same as in Fig. 3b.

To improve the description of the experimental data we tried the following approximating function [16]

$$S(E \text{ in keV}) = S_0 + S_1 E + S_2 E^2 \tag{12}$$

but did not succeed at this very low energy region.

In what follows we implement the parametrization of the calculated S-factor according to the expression (12) with $S_0 = 0.12133\text{E}00$ keV·b, $S_1 = -0.12718\text{E}{-}04$ b, $S_2 = 0.73463\text{E}{-}05$ b·keV^{-1} for the energy range up to 150 keV in c.m. We found the value χ^2 to be 0.31 within 1% precision of the theoretical S-factor. The result is shown by the dashed curve 2 in Fig. 4 and is consistent with experimental data in the previously mentioned energy region.

Experimental data shown by solid circles in Fig. 4 can be approximated by the Breit-Wigner type function

$$S(E) = a_1 + \frac{a_2}{(E - a_3)^2 + a_4^2/4} \tag{13}$$

with the following parameters $a_1 = 0.11413$, $a_2 = 7370.5$, $a_3 = 189.78$, $a_4 = 313.92$ (the energy is given in keV in c.m.). The results of this parametrization is shown by the solid curve 3 in Fig. 4, χ^2 is equal to 0.1 at 19% of experimental errors. At zero energy, this parametrization gives $S(0)$ = 0.236 keV·b. This form of parametrization at a resonance energy of 190 keV leads to a width of 314 keV, which almost coincides with the $3/2^+$ resonance parameters [18], given above.

We apply the ordinary χ^2 statistics as usually was done in [31,32] and defined as

$$\chi^2 = \frac{1}{N}\sum_{i=1}^{N}\left[\frac{S^a(E_i) - S^c(E_i)}{\Delta S^c(E_i)}\right]^2 = \frac{1}{N}\sum_{i=1}^{N}\chi_i^2.$$

Here S^c is the original, i.e. calculated and S^a is an approximate S-factor for the i-th energy, ΔS^c is the error of the original S-factor, which was usually taken equal to 1%, and N is the number of points in the summation in the expression. As the original S-factor its experimental or calculated values shown by the solid circles or the solid curve 4 in Fig. 4 are used, and the approximated S-factor is obtained on the basis of expressions (11) and (12).

We also use parametrization (12) for the calculation of the S-factor in the energy range up to 0.9 MeV c.m. and obtained the following parameters: $a_1 = 0.43449\text{E}{-}01$, $a_2 = 0.41439\text{E}{+}04$, $a_3 = 0.23046\text{E}{+}03$, $a_4 = 0.20604\text{E}{+}03$. Fig. 4 with curve 3 illustrates the quality of this procedure at $\chi^2 = 7.7$ at 1% error. At 6 keV in the c.m. or zero energy the value of the approximated S-factor (12) is 0.11 keV·b. The parametrization leads to a resonant energy of 230 keV at a width of 206 keV, which also in a good agreement with the data reported by [18]. Let us note that results of calculations for the S-factor presented in Fig. 4a are obtained using a parametrization of the potentials given in Table 4 in contrast to our previous calculations [50] and in a different range of energy.

4.3. Screening effects

The screening effects in plasma in laboratory as well as astrophysical conditions are discussed in detail in review [55]. Let us focus on the key points that can be applied to the reaction under consideration. The following relations for the cross sections and, accordingly, for the S-factors, are the generally accepted approximation for the estimation of electron screening

$$\frac{\sigma_s(E)}{\sigma_b(E)} = \frac{S_s(E)}{S_b(E)} = \frac{E}{E + U_e}\exp(\pi\eta U_e/E).$$

Here $\sigma_s(E)$ is the electron-screened cross section, $\sigma_b(E)$ is a cross bare nuclei, and U_e is a constant electron screening potential energy. The Sommerfeld parameter is $\eta = (Z_1 Z_2/\hbar c)\sqrt{\mu c^2/2E_{\text{cm}}}$. The value of U_e can be calculated analytically (*the adiabatic approximation*), or determined experimentally.

In our case, the ^{3}He(^{2}H, p)^{4}He process is of interest, since it has a common initial channel with the reaction under consideration ^{3}He(^{2}H, γ)^{5}Li. For this initial channel $U_e = 120$ eV is the adiabatic limit value [55]. It should be noted that for different experimental conditions U_e has a different value. So in [25] the direct measurements give the values $U_e = 219 \pm 7$ eV for ^{3}He(^{2}H, p)^{4}He and $U_e = 109 \pm 9$ eV for ^{2}H(^{3}He, p)^{4}He. Thus, for the same reaction the difference is almost two fold. In a later experimental work [56], the screening effect turned out to be negligible. For some reason, the reference [56] was not included in the review [55], in

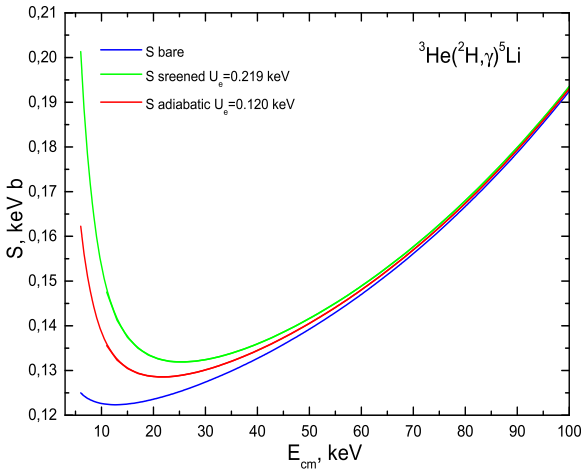

Fig. 5. The screening effects for the astrophysical S-factor of the ^{3}He(^{2}H, γ)^{5}Li capture.

which the significance of electron screening for astrophysical plasma is discussed in terms of *pycnonuclear ignition*.

Fig. 5 illustrates the possible effect of electron screening for the process we are considering. The value of S_b corresponds to the curve 1 in Fig. 5, e.g. $U_e = 0$, and the minimum value for E_{cm} is 6 keV. It is clearly seen from Fig. 5 that the screening effect strongly depends on the value of U_e, and it varies from 65 to 219 keV in different works [55]. Obviously, until this value is determined quite accurately, it is also impossible to determine the impact of the screening effect. Therefore, it is not taken into account in calculating the reaction rate.

4.4. Reaction rates

The reaction rate in cm^3 mol^{-1} s^{-1} units is usually defined as [46]

$$N_A\langle\sigma v\rangle = 3.7313 \cdot 10^4 \mu^{-1/2} T_9^{-3/2} \int_0^\infty \sigma(E) E \exp(-11.605 E/T_9) dE,$$

where the energy E is taken in MeV, total cross section $\sigma(E)$ in μb, the reduced mass μ in amu, and temperature T_9 in 10^9 K [46]. To calculate this, integral 10^4 points of the theoretical cross section were taken in c.m. energy range from 6 keV to 10 MeV.

In Fig. 6 the solid curve shows the results of our calculations for reaction rate of the ^{3}He(^{2}H, γ)^{5}Li capture on the GS at T_9 from 0.003 to 10, which corresponds to the same curve in Figs. 3 and 4. It should be borne in mind that the reaction rate was obtained from the calculated cross section, which slightly differs from the experimental cross section.

The dots in Fig. 6 display the results of Ref. [23], which have a larger value of reaction rate. This is due to the strong decrease of our calculated total cross sections in the energy range 0.5 ± 1.0 MeV and insufficiently accurate description of the cross sections at energies 1–6 MeV. This reaction rate is more than an order of magnitude higher than the rate of the ^{3}He(^{2}H, γ)^{5}Li reaction considered here.

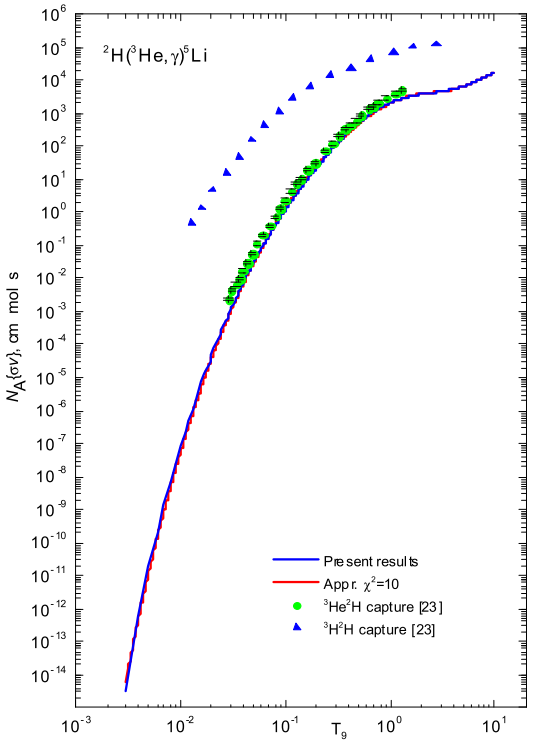

Fig. 6. Reaction rate of the ^{3}He(^{2}H, γ)^{5}Li radiative capture. Theoretical curves obtained using the potential (4) with the parameters from Tables 3 and 4. An explanation of the parameterization functions is given in text. Dots (●) are the results from Ref. [23] for the ^{3}He(^{2}H, γ)^{5}Li capture, the triangles (▲) are the results of [23] for the ^{3}H(^{2}H, γ)^{5}He capture.

The calculated reaction rate shown on Fig. 6 was approximated in the range 0.03–10.0 T_9 as follows [12]

$$N_A\langle\sigma v\rangle = 20986.49/T_9^{2/3}\cdot\exp\left(-7.13006/T_9^{1/3}\right)\cdot\left(1.0+126.7438\cdot T_9^{1/3}\right.$$
$$\left.-28.83194\cdot T_9^{2/3}+65.13721\cdot T_9+47.34928\cdot T_9^{4/3}-22.35306\cdot T_9^{5/3}\right)$$
$$-4.94921\cdot 10^6/T_9^{1/2}\exp\left(-8.34422/T_9^{1/2}\right). \quad (14)$$

The resulting curve is shown as dashed one in Fig. 6, χ^2 is equal to 10. In the approximation, the calculated points shown in Fig. 6 with a solid curve were used. To estimate the χ^2 the error was taken to be 1%.

5. Alternative way of ^{6}Li nuclei formation at the BBN

Furthermore, we consider a possible scenario of thermonuclear astrophysical processes involving a short-lived ^{5}Li isotope, which is formed as a result of the ^{3}He(^{2}H, γ)^{5}Li reaction. In any plasma, when a short-lived ^{5}Li isotope is formed the probability of neutron capture followed by the formation of a stable ^{6}Li is not zero. At first, such a chain of two reactions allows us to overcome the mass disruption at $A = 5$, leading to a stable nucleus with $A = 6$. Secondly, the reaction ^{5}Li(n,γ)^{6}Li leads to an additional ^{6}Li formation channel, which can be considered for the explanation of the prevalence ^{6}Li.

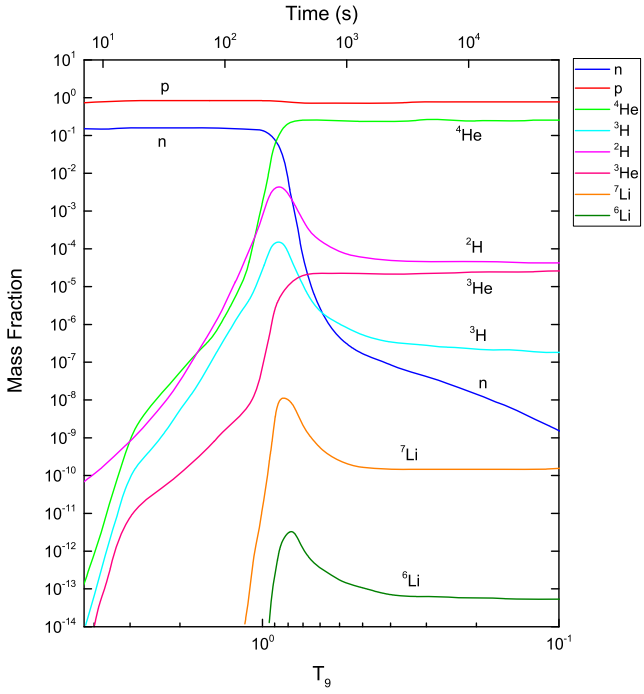

Fig. 7. Nuclei formation mass fractions in the Big Bang thermonuclear processes.

We will describe below a possible and, as it seems to us, a new scenario for the synthesis of the ^{6}Li isotope in astrophysical processes and, first of all, at the Big Bang. It is required to find out whether there is a "temperature window" that would allow such an amount of ^{6}Li to be accumulated during the Big Bang, which could change the balance of ^{6}Li, including in the region of a sharp drop in the number of neutrons at $T_9 < 1$. The general dynamics of the synthesis of the light and lightest elements within the conditions of the standard Big Bang is represented by a graph of the participating particles fractions, shown in Fig. 12 in work [57]. This graph is adapted here for our purposes and shown in Fig. 7. It displays a sharp drop in the number of neutrons at $T_9 < 1$, which turn out to be bound in heavier nuclei. The number of such nuclei, for example, ^{4}He and ^{3}He, increases strongly at lower temperatures, since the energy of the interaction becomes so small for their breakdown.

We present below two reactions of radiative capture, which are usually considered as candidates for the role of the ^{6}Li formation processes in the Big Bang and compare their rates with each other. It is believed that the radiative capture reaction

$$^4\mathrm{He} +^2 \mathrm{H} \rightarrow {}^6\mathrm{Li} + \gamma \tag{15}$$

is one of the source of ^{6}Li in the Big Bang, i.e., in the temperature range 50–400 keV [55]. The relationship between temperature and energy is assumed to be 1.0 $T_9 = 86.17$ keV [46].

Therefore, the energy range from 50 up to 400 keV corresponds approximately to the temperature range 0.6–4.5 T_9. A feature of this process is the forbiddance of the "strong" dipole $E1$ transition by the selection rules. So the reaction is due to the $E2$ transition, excepting the lowest energies, where the $E1$ process makes an appreciable contribution to the overall picture. As a result, the cross section of reaction (15) is only a few nanobarns and sharply decreases with

Table 6
The parameters of the expression (18) for parameterizing the data in Fig. 8.

a_1	a_2	a_3	a_4	a_5	a_6	a_7	a_8	a_9
−0.66815E+02	0.92167E+03	0.18011E+01	0.64950E+01	−0.26955E+01	−0.31659E+00	0.16969E+00	0.90199E+04	0.60666E+01

b_1	b_2	b_3	b_4	b_5
0.63402E+00	0.65888E+00	0.22340E+01	0.15001E+01	0.62889E+00

energy decreasing due to the Coulomb barrier. The specified parametrization of this reaction rate is given by Trezzi et al. [58]

$$N_A\langle\sigma v\rangle = 20.07T_9^{-2/3}\exp\left(-7.47T_9^{-1/3}\right)\left(1.0 - 4.709T_9^{1/3} + 17.219T_9^{2/3} - 23.839T_9 + 19.27T_9^{4/3} - 3.752T_9^{5/3}\right) + 65.409T_9^{-3/2}\exp\left(-7.565T_9^{-1}\right). \quad (16)$$

This parametrization is used for comparison of the rates of radiative capture processes under consideration. There are no fundamental differences between (16) and similar parametrization from the survey [12].

Theoretical and experimental aspects of the ^{6}Li formation problem in the ^{4}He+^{2}H $\to$ ^{6}Li + γ reaction (Lithium problem) are discussed in detail in one of the most recent publication [59]. The authors believe that despite all the efforts of accurate theoretical calculations, even when the tensor component of the ^{4}He^{2}H forces [60] is taken into account, it is possible to overcome the discrepancy with the experimentally established prevalence of ^{6}Li/H $\sim 1.7 \cdot 10^{-14}$ only within $\sim$20%.

Therefore, as an additional source of ^{6}Li formation in the Big Bang, the reaction [61]

$$^3\mathrm{He} + {}^3\mathrm{H} \to {}^6\mathrm{Li} + \gamma. \quad (17)$$

was considered. However, we could not find the parametrization of the rate of such a reaction or its theoretical calculations. In order to calculate the rate of this reaction, we perform the parametrization of its total cross sections. We use polynomial form with the Breit-Wigner term

$$\sigma(E) = a_1 + \frac{a_2}{(E-a_3)^2 + a_4^2/4} + a_5E^{b_1} + a_6E^{b_2} + a_7E^{b_3} + a_8/E^{b_4}\exp\left(-a_9/E^{b_5}\right). \quad (18)$$

Basic experimental data were taken from [62]. Here we give 23 points for the total cross sections and we took one more point from [61] at 81 keV in c.m. All experimental data are shown in Fig. 8. The parametrization (18) with the parameters given in Table 6 leads to $\chi^2 = 0.4$, and the corresponding result is shown in Fig. 8 with the solid curve 1.

All parameters given in Table 6 are varied independently to obtain a minimum value of χ^2. From Table 6 we see that the power of b_4 is 3/2, as is usually assumed in similar calculations [12], the powers of b_1, b_2 and b_5 are close to 2/3, and the power of b_3 is approximately equal 2. But if we take powers, excepting the one of b_4, to be equal to these integers, this leads to an increase in χ^2 of up to 1.4. Moreover, if we perform additional variation of the remaining parameters a_i, then, despite the small value of $\chi^2 = 0.3$, the approximated cross section becomes negative even at energies below 50 keV, which strongly affects the shape of the reaction rate.

Therefore, in order to calculate the reaction rate, we used the parametrization (18) with the parameters given in Table 6. This parametrization leads to negative cross sections at energies below 5 keV, therefore the calculation of the cross section is limited by this energy value. In Fig. 8, the dashed curve 2 shows the cross section obtained from the parameterization (18) and

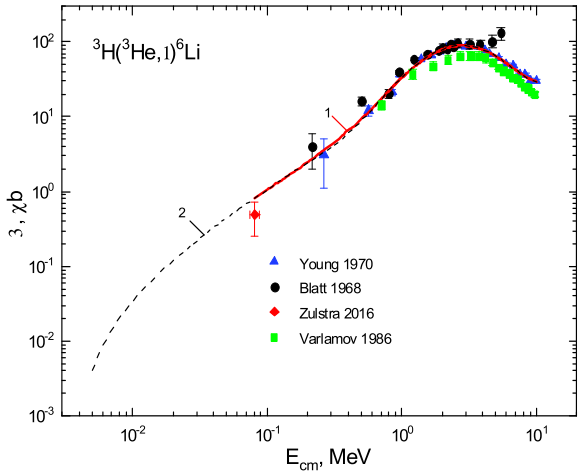

Fig. 8. Radiative ^{3}H(^{3}He, γ)^{6}Li capture cross sections. The experimental data are as follows: [63] – ●, [62] – ▲, [61] – ◆. For comparison, the results of [64] are given by ■. Solid curves show different parameterizations (18) used in the present paper.

calculated in the energy range from 0.005 to 10 MeV, which is directly used later for calculations of the rate of reaction (17).

Furthermore, another reaction can be considered. The following process can be estimated as an additional ^{6}Li synthesis channel

$$n + {}^5\mathrm{Li} \to {}^6\mathrm{Li} + \gamma. \tag{19}$$

Obviously, a direct measurement of the cross section of this process is impossible. However, according to detailed balance, this cross section can be estimated from data for the photodisintegration reaction ^{6}Li(γ, n)^{5}Li with binding energy $E_{51} = 5.67$ MeV. The arguments in favor of the fact that the cross section of the reaction (19) can be significant is the absence of a Coulomb barrier, and also a centrifugal barrier, since a "strong" dipole $E1$ transition is realized from scattering S-waves.

For further analytical calculations of the reaction (19) rate two variants of the cross section parameterization were obtained. In Fig. 9a the solid curve shows the following version of the parameterization

$$\sigma(E) = a_1 + \frac{a_2}{(E - a_3)^2 + a_4^2/4} + a_5 E \tag{20}$$

with the parameters $a_1 = -0.62090\mathrm{E}{-}01$, $a_2 = 0.10927\mathrm{E}{+}03$, $a_3 = 0.64065\mathrm{E}{+}01$, $a_4 = 0.79845\mathrm{E}{+}01$, $a_5 = 0.27650\mathrm{E}{+}00$ with $\chi^2 = 0.023$.

These parameters were obtained as a parametrization of the data of Ref. [64] taken from Ref. [65] and shown with the solid circles in Fig. 9. However, this parameterization does not properly describe the behavior of the cross section at thermal energy. The cross section reaches a plateau with a value of 1.9 microbars for any, arbitrarily low energy. Since the thermal cross section for this reaction was not measured by anyone, we can assume for it the value of 40 mb, as for ^{7}Li [66]. The use of this data on thermal neutrons for ^{7}Li is completely justified, because in the ground state this nucleus has the same quantum numbers $J^\pi = 3/2^-$ as ^{5}Li, while it is reasonable, for the first estimate, to assume that they have similar rms sizes.

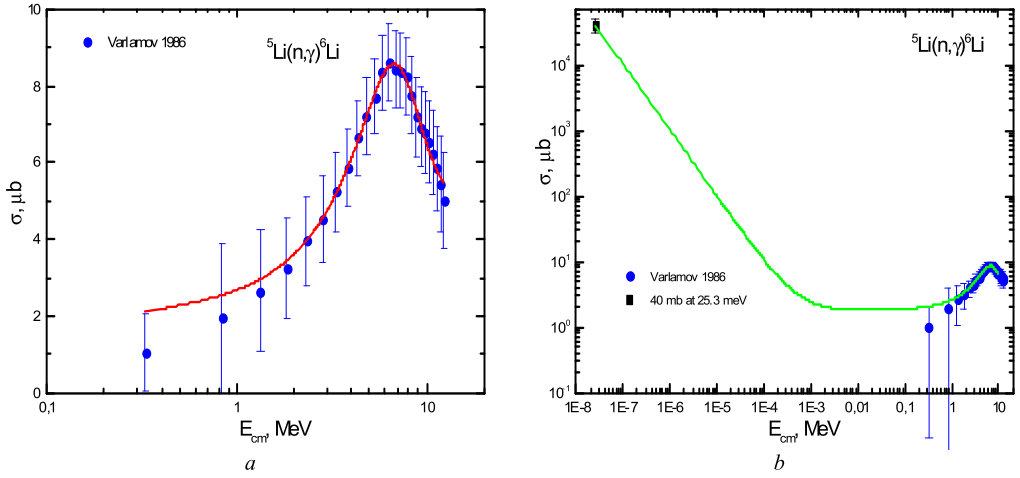

Fig. 9. The cross section for the radiative ^{5}Li(n, γ)^{6}Li capture based on the data for ^{6}Li(γ, n)^{5}Li photodisintegration. The experimental data are taken from Ref. [64]. Curves are obtained using the parametrization of the present work: a – without reference to thermal cross sections σ_{th}; b – with reference to σ_{th} for ^{7}Li.

For a correct description of the thermal cross sections, it is required to change the form of the parametrization (20) as

$$\sigma(E) = a_1 + \frac{a_2}{(E - a_3)^2 + a_4^2/4} + a_5 E + a_6/\sqrt{E} + a_7/E \tag{21}$$

with parameters $a_1 = -0.62090\text{E}{-}01$; $a_2 = 0.10823\text{E}{+}03$; $a_3 = 0.63957\text{E}{+}01$; $a_4 = 0.79517\text{E}{+}01$; $a_5 = 0.27950\text{E}{+}00$; $a_6 = -0.14339\text{E}{-}01$; $a_7 = 0.10142\text{E}{-}02$ and $\chi^2 = 0.0216$. The green curve in Fig. 9b is obtained from the parametrization (20), taking into account the reference to the thermal neutron capture cross section. Hence one can see that the parametrized cross section well conveys the results of Ref. [64] and describes the data at the thermal energy. However, one must bear in mind that at medium energies below the data given in Ref. [64], there is a "plateau", which is not characteristic of such cross sections [32].

Furthermore, in Fig. 10 one can see the reaction rates of some radiative capture processes which can lead to synthesis of ^{6}Li or can be an intermediate stage for its synthesis. The solid curve 1 shows the results for the capture reaction rate of ^{3}H(^{3}He, γ)^{6}Li obtained on the basis of our the parameterization (18). Let us once again pay attention to the fact that such a parametrization leads to negative cross sections at energies below 5 keV. Therefore, the cross sections are cut off at this energy, which apparently leads to a more rapid decrease in the reaction rates at low temperatures. The solid curve 2′ shows the rate of the neutron capture on ^{5}Li for the case of the parametrization (19), and the curve 2 – for the parameterization (20), which makes it possible to describe the cross sections at thermal energies.

It is easy to see an increase in the reaction rate at low temperatures if we take into account the thermal cross sections for the ^{5}Li(n, γ)^{6}Li capture. The curve 3 is the rate of the capture ^{4}He(^{2}H, γ)^{6}Li reaction, obtained from the parametrization (16) of [58]. The curve 4 shows our calculations of the rate of the ^{3}He(^{2}H, γ)^{5}Li capture reaction, which can be parametrized with the expression (13) from the previous section.

As follows from Fig. 10, the rate of the "priority" reaction $^4\text{He} + {}^2\text{H} \rightarrow {}^6\text{Li} + \gamma$ is less than all the others. Therefore, the question about the role of the $^3\text{He} + {}^3\text{H} \rightarrow {}^6\text{Li} + \gamma$ process, as a

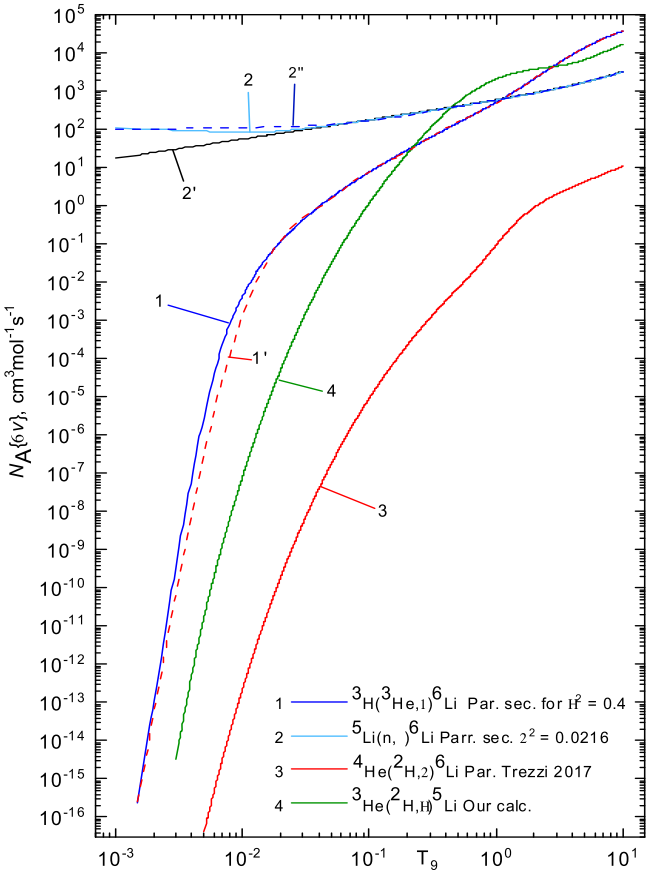

Fig. 10. Different radiative capture reactions rates.

possible candidate for amplifying the ^{6}Li yield arose. The answer is contained in the comparison of the reaction rates presented in Fig. 10 and particles fractions in the process of BBN in Fig. 7. Against the background of a large fraction of alpha particles, the deuterium fraction decreases with decreasing temperature. The synthesis of ^{3}He is accelerated and to some extent compared with the amount of ^{2}H, starting from $T_9 \sim 1$. In the same region, a maximum is observed for tritium ^{3}H, the fraction of which, however, sharply decreases with time. As a result, the conclusions of [61] on the minor contribution of this reaction in comparison with (15) are understandable.

It follows from Fig. 10 that the reaction rate of the ^{5}Li synthesis (curve 4) with the participation of deuterium and ^{3}He at $T_9 \sim 1$ is comparable and even greater than the process (15), and the deuterium fraction exceeds the tritium fraction by one order. In Fig. 10 it is clearly shown that the rate of reaction ^{5}Li$(n, \gamma)^6$Li is greater than for ^{3}H$(^3$He, $\gamma)^6$Li and ^{3}He$(^2$H, $\gamma)^5$Li, and even greater than for ^{4}He$(^2$H, $\gamma)^6$Li reactions. Therefore, it can be assumed that in the $T_9 \sim 1$ region, which corresponds to a large neutron concentration, we can expect the real contribution of the reaction $n + {}^5\text{Li} \to {}^6\text{Li} + \gamma$ to the ^{6}Li synthesis.

Now we give the parametrizations of ^{5}Li$(n, \gamma)^6$Li and ^{3}H$(^3$He, $\gamma)^6$Li capture reactions rates. In the first case, it was possible to find only a polynomial form of the parametrization

Table 7
The parameters for expression (22).

a_1	a_2	a_3	a_4	a_5	a_6	a_7
100.2674	717.7027	−296.7566	93.84265	−15.13806	1.2058	−0.0374

Table 8
The parameters for expression (23).

a_1	a_2	a_3	a_4	a_5	a_6	a_7	a_8
74.07273	1.8375	4.95476	0.4065	2183.953	−1.69893	−3714.616	−1.56543
a_9	a_{10}	a_{11}	a_{12}	a_{13}	a_{14}	a_{15}	a_{16}
907.838	3.00098	−324.5072	3.31375	11793.31	2.28774	2.48388	0.53456

$$N_A \langle \sigma v \rangle = \sum_{i=1}^{N} a_i E^{i-1} \tag{22}$$

with the parameters from Table 7. This form at $N = 7$ leads to $\chi^2 = 3.0$. Here and below, for calculations of χ^2, the error was assumed to be 1%. The results of the approximation are shown in Fig. 10 with the dashed curve $2''$.

To parameterize the rate of the second reaction, another form

$$\begin{aligned} N_A \langle \sigma v \rangle = {} & a_1 / T_9^{a_2} \exp\left(-a_3 / T_9^{a_4}\right)\left(1.0 + a_5 T_9^{a_6} + a_7 T_9^{a_8} + a_9 T_9^{a_{10}} + a_{11} T_9^{a_{12}}\right) \\ & + a_{13} / T_9^{a_{14}} \exp\left(-a_{15} / T_9^{a_{16}}\right) \end{aligned} \tag{23}$$

was used which leads to $\chi^2 = 32.4$. The results of the approximation are shown in Fig. 10 with the dashed curve $1'$ with parameters given in Table 8. As seen from Fig. 10, the rate of the ^{3}H(^{3}He, γ)^{6}Li capture reaction has an unusual form. Perhaps this is a consequence of the overestimated cross section obtained from the parametrization (18) in the low-energy region. Therefore, in expression (23), it is required to vary not only the coefficients of the T_9 powers, but also the values of the powers themselves.

Based on the obtained results, a more consistent evaluation of the role of the $n + {}^5\text{Li} \to {}^6\text{Li} + \gamma$ process in the BBN and in stars is desirable in the future. For this purpose, all necessary cross section parameterizations and reaction rates are obtained in this paper. In addition, our simple estimates based on the mass fraction distribution shows qualitatively that the role of the $n + {}^5\text{Li} \to {}^6\text{Li} + \gamma$ reaction requires a further study for astrophysical processes in conditions of high neutron concentration, which have a different temperature regime compared to the BBN.

We present calculations for the total cross sections, astrophysical S-factor, and reaction rates for ^{3}He(^{2}H, γ)^{5}Li radiative capture in the framework of the potential cluster model with forbidden states using a single channel approach. We show that the integral characteristics of ^{3}He(^{2}H, γ)^{5}Li radiative capture can be reproduced with very high accuracy. Our results are promising and pave the way for further microscopic analyses of this process. However, it is well known that the ^{3}He(^{2}H, p)^{4}He and ^{3}H(^{2}H, n)^{4}He) reactions are strongly dominant. We are well aware of the classical works within the method of resonating groups on the investigation of the $\alpha + N$ scattering channels taking into account the coupled-channels for five-nucleon systems. This formalism found wide acceptance following its application to calculations of various polarization characteristics [67]. Indeed, there are indications of very subtle effects associated with

channels coupling for polarization characteristics. Today the Gaussian expansion method to accurately solve the Schrödinger equations, which includes heavy calculations for bound, resonant and scattering states of three- to five-body systems (see review: [68] and references) is used for coupled-channels calculations. Our calculations can be further improved by including additional $\alpha + N$ channels by performing coupled-channels calculations. The description of the five-nucleon system using the potential model within the Schrödinger equations with modern nucleon-nucleon potentials is a challenging issue and beyond the scope of the present research.

One should pay attention to the fact that the variation in the data on integral sections, which we use for astrophysical calculations, is quite large. In Section 2 we did our best to reasonably and maximally coordinate both the total cross sections and yields of the processes. We relied on this compilation of the data that served as a criterion for the reliability of our calculations. One can see that the experimental data can be reproduced within a single-channel approach. In our opinion the coupled-channels calculations will not dramatically change the resulting pattern.

In this paper we make the assumption related to the existence of the two step mechanism ^{3}He(^{2}H, γ)^{5}Li $\rightarrow$ ^{5}Li(n, γ)^{6}Li in formation of ^{6}Li as one of the options to address the lithium abundance within the BBN model. The role of short-lived isotopes in astrophysical thermonuclear processes is quickly becoming a popular subject of experimental and theoretical research, so in this pioneering work, we tried to identify some problematic aspects of these calculations regarding the lack of information in the literature for the considered processes. In addition, a role of two-step processes, which are extremely difficult to study in laboratory conditions, but which, nevertheless, occur in natural plasma, requires clarification. These processes either make a certain contribution to the scenario of stellar plasma evolution as a whole, or their role should be considered insignificant. This question is open, and we have demonstrated one of ways to address its solution.

6. Conclusion

In conclusion, we note that the main goal of our studies is to determine the role of the ^{3}He(^{2}H, γ)^{5}Li radiative capture reaction in the balance of processes involving deuterons that occur under natural and laboratory conditions in plasma. This reaction was not considered in the review [12], which presents the parameterization of reaction rates involving light and lightest nuclei. The contribution of this work to this important compilation consists in calculating the rate of the ^{3}He(^{2}H, γ)^{5}Li process based on a certain nuclear model and its corresponding parametrization (13).

Nuclear physics aspects

Comparatively simple-channel model representations (namely, the use of MPCM in this work) succeeded to obtain the theoretical results in general agreement with the available experimental data for the S-factor or total cross section of the radiative ^{3}He(^{2}H, γ)^{5}Li capture. The larger value of minimum in the cross sections at energies 0.4 ± 2 MeV, in comparison with the experiment, can be due to the fact that we do not take into account any additional electromagnetic transitions, in spite of we took into account 12 such processes. However, there may be another explanation. In the experimental data for capture on the GS a contribution from the transition to FES is present. All the main available experimental data, reviewed in Sec. 2, were obtained and published about 45 to 60 years ago and obviously require clarification.

Nuclear astrophysics aspects

From the point of view of further application of the results obtained here in astrophysical problems, we can indicate the following:

1. Simple parametrizations of the considered radiative ^{5}Li(n, γ)^{6}Li and ^{3}H(^{3}He, γ)^{6}Li capture reactions cross sections and their rates are obtained.
2. The rates of these two processes and the rate of the ^{3}He(^{2}H, γ)^{5}Li capture reaction considered here are compared.
3. The possible contribution of the neutron capture on ^{5}Li to the formation of a stable ^{6}Li is considered.
4. It has been shown qualitatively that the neutron capture on ^{5}Li formed at ^{3}He(^{2}H, γ)^{5}Li capture in the temperature range of the order of $1.0T_9$ at the BBN, can make a significant contribution to the processes of primary accumulation of a stable ^{6}Li.

On the basis of all results obtained here it is clear that now it is required to make quantitative calculations of the contribution of such reactions to the accumulation of the ^{6}Li nucleus at BBN in stars and other astrophysical processes.

Acknowledgements

This work was supported by the Grant of Ministry of Education and Science of the Republic of Kazakhstan through the program BR05236322 “Study reactions of thermonuclear processes in extragalactic and galactic objects and their subsystems” in the frame of theme “Study of thermonuclear processes in stars and primordial nucleosynthesis” through the Fesenkov Astrophysical Institute of the National Center for Space Research and Technology of the Ministry of Defence and Aerospace Industry of the Republic of Kazakhstan (RK).

References

[1] C.A. Barnes, D.D. Clayton, D.N. Schramm, Essays in Nuclear Astrophysics. Presented to William A. Fowler, Cambridge University Press, Cambridge, 1982, p. 562; http://www.cambridge.org/us/academic/subjects/physics/particle-physics-and-nuclear-physics/essays-nuclear-astrophysics.
[2] J.R. Lierrer, et al., Rev. Sci. Instrum. 63 (1992) 4847.
[3] S.E. Sharapov, T. Hellsten, V.G. Kiptily, Nucl. Fusion 56 (2016) 112021.
[4] J.M. Blair, et al., Phys. Rev. 96 (1954) 1023.
[5] L. Kraus, et al., Nucl. Phys. A 109 (1968) 593.
[6] W. Del Bianco, et al., Can. J. Phys. 46 (1968) 1585.
[7] W. Buss, et al., Nucl. Phys. A 112 (1968) 47.
[8] H. Schroder, W. Mausberg, Z. Phys. 235 (1970) 234.
[9] H.R. Weller, M.J. Balbes, Nucl. Instrum. Methods Phys. Res., Sect. A 402 (1998) 428.
[10] M.J. Balbes, et al., Phys. Rev. C 49 (1994) 912.
[11] V.G. Kiptily, F.E. Cecil, S.S. Medley, Plasma Phys. Control. Fusion 48 (2006) R59.
[12] G.R. Caughlan, W.A. Fowler, At. Data Nucl. Data Tables 40 (1988) 283.
[13] EXFOR, https://www-nds.iaea.org/exfor/exfor.htm, 2013.
[14] C. Casella, et al., Nucl. Phys. A 706 (2002) 203.
[15] G.J. Schimd, et al., Phys. Rev. C 56 (1997) 2565.
[16] R. Canon, et al., Phys. Rev. C 65 (2002) 044008.
[17] F.E. Cecil, H. Liu, J.S. Yan, Vacuum 44 (1993) 181.
[18] D.R. Tilley, C.M. Cheves, J.L. Godwin, G.M. Hale, H.M. Hofmann, J.H. Kelley, C.G. Sheu, H.R. Weller, Nucl. Phys. A 708 (2002) 3; Updated data for energy levels of light nuclei $A = 5$, 2017; http://www.tunl.duke.edu/nucldata/ourpubs/05_2002.pdf.

[19] F. Ajzenberg-Selove, Nucl. Phys. A 490 (1988) 1.
[20] H.T. King, W.E. Meyerhof, R.G. Hirko, Nucl. Phys. A 178 (1972) 337.
[21] Fundamental Physical Constants, 2010, CODATA, http://physics.nist.gov/cgi-bin/cuu/Value?mudlsearch_for=atomnuc!.
[22] Nuclear Wallet Cards, http://cdfe.sinp.msu.ru/services/ground/NuclChart_release.html, 2014.
[23] F.E. Cecil, D.M. Cole, F.J. Wilkinson, Nucl. Instrum. Methods Phys. Res., Sect. B 10/11 (1985) 411.
[24] F.E. Cecil, D.M. Cole, R. Philbin, Phys. Rev. C 32 (1985) 690.
[25] M.A. Aliotta, et al., Nucl. Phys. A 690 (2001) 790.
[26] F.S. Chwieroth, et al., Phys. Rev. C 8 (1973) 938.
[27] D. Kurath, Phys. Rev. 47 (1993) 1306.
[28] M. Tanifuji, H. Kameyama, Nucl. Phys. A 602 (1996) 1.
[29] R.F. Wagner, C. Werntz, Phys. Rev. C 4 (1971) 2.
[30] P. Navratil, S. Quaglioni, Phys. Rev. Lett. 108 (2012) 042503.
[31] S.B. Dubovichenko, Thermonuclear Processes in Stars and Universe, second English edition, revised and expanded, Scholar's Press, Saarbrucken, 2015, 332 pp. https://www.scholars-press.com/catalog/details/store/gb/book/978-3-639-76478-9/Thermonuclear-processes-in-stars.
[32] S.B. Dubovichenko, Radiative neutron capture and primordial nucleosynthesis of the Universe, in: Selected Methods for Nuclear Astrophysics, fifth Russian edition revised and expanded, Lambert Academy Publ. GmbH&Co. KG., Saarbrucken, 2016, 496p. https://www.ljubljuknigi.ru/store/ru/book/radiative-neutron-capture/isbn/978-3-659-82490-6, 2019. (Accepted to press in de Gruyter in 2019).
[33] S.B. Dubovichenko, A.V. Dzhazairov-Kakhramanov, Astrophys. J. 819 (2016) 78.
[34] S.B. Dubovichenko, A.V. Dzhazairov-Kakhramanov, Ann. Phys. 524 (2012) 850.
[35] S.B. Dubovichenko, A.V. Dzhazairov-Kakhramanov, Nucl. Phys. A 941 (2015) 335.
[36] S.B. Dubovichenko, A.V. Dzhazairov-Kakhramanov, N.V. Afanasyeva, Nucl. Phys. A 963 (2017) 52.
[37] S.B. Dubovichenko, A.V. Dzhazairov-Kakhramanov, Int. J. Mod. Phys. E 26 (2017) 1630009, and references here to our previous reviews.
[38] S.B. Dubovichenko, N.A. Burkova, Mod. Phys. Lett. A 29 (2014) 1450036.
[39] S.B. Dubovichenko, et al., Mod. Phys. Lett. A 29 (2014) 1450125.
[40] T. Mertelmeir, H.M. Hofmann, Nucl. Phys. A 459 (1986) 387.
[41] P. Descouvemont, et al., AIP Adv. 4 (2014) 041011.
[42] P. Descouvemont, et al., Nuclear reactions in stars: theoretical and experimental aspects, in: The Universe Evolution. Astrophysical and Nuclear Aspects, NOVA Sci. Publ., New-York, 2013, pp. 1–48.
[43] V.G. Neudatchin, et al., Phys. Rev. C 45 (1992) 1512.
[44] V.G. Neudatchin, A.A. Sakharuk, S.B. Dubovichenko, Few-Body Syst. 18 (1995) 159.
[45] S.B. Dubovichenko, A.V. Dzhazairov-Kakhramanov, Phys. Part. Nucl. 28 (1997) 615.
[46] C. Angulo, et al., Nucl. Phys. A 656 (1999) 3.
[47] Chart nucl. shape & size param. ($0 \leq Z \leq 14$), 2015, http://cdfe.sinp.msu.ru/cgi-bin/muh/radchartnucl.cgi?zmin=0&zmax=14&tdata=123456.
[48] C. Itzykson, M. Nauenberg, Rev. Mod. Phys. 38 (1966) 95.
[49] B. Jenny, et al., Nucl. Phys. A 337 (1980) 77.
[50] S.B. Dubovichenko, N.A. Burkova, A.V. Dzhazairov-Kakhramanov, A.S. Tkachenko, Russ. Phys. J. 60 (2017) 935.
[51] S.B. Dubovichenko, Phase Shifts Analysis in Nuclear Astrophysics, Lambert Academy Publ. GmbH&Co. KG., Saarbrucken, 2015, 368p. (in Russian).
[52] G.R. Plattner, R.D. Viollier, Nucl. Phys. A 365 (1981) 8.
[53] W.A. Fowler, G.R. Caughlan, B.A. Zimmerman, Annu. Rev. Astron. Astrophys. 13 (1975) 69.
[54] P.J. Mohr, B.N. Taylor, Rev. Mod. Phys. 77 (1) (2005) 1.
[55] C.A. Bertulani, T. Kajino, Prog. Part. Nucl. Phys. 89 (2016) 56.
[56] M. Barbui, W. Bang, A. Bonasera, et al., Phys. Rev. Lett. 111 (2013) 082502.
[57] A. Coc, et al., Astrophys. J. 744 (2012) 158.
[58] D. Trezzi, et al., Astropart. Phys. 89 (2017) 57.
[59] A. Grassi, G. Mangano, L.E. Marcucci, O. Pisanti, Phys. Rev. C 96 (2017) 045807.
[60] S.B. Dubovichenko, Phys. At. Nucl. 61 (1998) 162.
[61] A.B. Zylstra, H.W. Herrmann, M.G. Johnson, et al., Phys. Rev. Lett. 117 (2016) 035002.
[62] A.M. Young, S.L. Blatt, R.G. Seyler, Phys. Rev. Lett. 25 (1970) 1764.
[63] S.L. Blatt, et al., Phys. Rev. 176 (1968) 1147.
[64] V.V. Varlamov, et al., CDFE/LI2, http://cdfe.sinp.msu.ru, 1986.

[65] Nuclear Reaction Database (EXFOR), http://cdfe.sinp.msu.ru/exfor/index.php, 2013.
[66] R.B. Firestone, Zs. Revay, Phys. Rev. C 93 (2016) 054306.
[67] K. Wildermuth, Y.C. Tang, Unified Theory of the Nucleus, Vieweg, Braunschweig, 1977, 389 p.
[68] E. Hiyama, M. Kamimura, Front. Phys. 18 (2018) 132106.